Article

High throughput LC-MS/MS proteomic analysis of a mouse model of Mesiotemporal lobe epilepsy predicts microglial activation underlying disease development

Vasiliki Bitsika, Venceslas Duveau, Julia Simon-Areces, William Mullen, Corinne Roucard, Manousos Makridakis, George Mermelekas , Pantelis Savvopoulos, Antoine Depaulis, and Antonia Vlahou

J. Proteome Res., **Just Accepted Manuscript** • DOI: 10.1021/acs.jproteome.6b00003 • Publication Date (Web): 08 Apr 2016

High throughput LC-MS/MS proteomic analysis of a mouse model of Mesiotemporal lobe epilepsy predicts microglial activation underlying disease development

AUTHOR NAMES

Vasiliki Bitsika [1], Venceslas Duveau [2], Julia Simon-Areces [3], William Mullen [4], Corinne Roucard [2], Manousos Makridakis [1], George Mermelekas [1], Pantelis Savvopoulos [1], Antoine Depaulis [3] and Antonia Vlahou [1]*

AFFILIATIONS

[1]Biotechnology Division, Biomedical Research Foundation, Academy of Athens, Greece

[2]SynapCell SAS, F-38700 La Tronche, France

[3]Inserm, U1216, Grenoble-Institut des Neurosciences, F-38000 Grenoble, France

[4]BHF Glasgow Cardiovascular Research Centre, University of Glasgow, Glasgow, UK

*Corresponding author:

Dr Vasiliki Bitsika

Biotechnology Division,

Biomedical Research Foundation, Academy of Athens, Greece

Soranou Efessiou 4, 11527, Athens Greece

0030-2106597485

vabitsika@bioacademy.gr

ABSTRACT

Uncovering the molecular mechanisms of Mesial temporal lobe epilepsy (MTLE) is critical to identify therapeutic targets. In this study, we performed global protein expression analysis of a kainic acid (KA) MTLE mouse model at various time-points (1d, 3d, 30d post KA injection -dpi), representing specific stages of the syndrome. High resolution liquid chromatography coupled to tandem mass spectrometry (LC-MS/MS), in combination to label-free protein quantification, using three processing approaches for quantification, was applied. Following comparison of KA versus NaCl-injected mice, 22, 53 and 175 proteins were differentially (statistically significant) expressed at 1, 3 and 30dpi respectively, according to all 3 quantification approaches. Selected findings were confirmed by multiple reaction monitoring LC-MS/MS. As a positive control, the astrocyte marker GFAP was found to be upregulated (3dpi:1.9 fold; 30dpi:12.5 fold), also verified by IHC. The results collectively suggest that impairment in synaptic transmission occurs even right after initial status epilepticus (1dpi), with neurodegeneration becoming more extensive during epileptogenesis (3dpi) and sustained at the chronic phase (30dpi), where also extensive glial and astrocyte–mediated inflammation is evident. This molecular profile is in line with observed phenotypic changes in human MTLE, providing the basis for future studies on new molecular targets for the disease.

KEYWORDS

Epilepsy, MTLE, Kainic acid, LC-MS/MS, proteomics

INTRODUCTION

The Mesio-Temporal Lobe Epilepsy (MTLE) syndrome is the most common form of intractable focal epilepsies. It is well accepted that most MTLE patients have experienced during early childhood an insult such as complex febrile seizures, head trauma, intracerebral infections or ischemia episodes[1, 2]. This initiating insult triggers cascades of molecular mechanisms over a period of several years during which no clinical symptoms are observed. This so-called "silent period" corresponds to the progressive development of epilepsy (i.e. epileptogenesis) ultimately leading to recurrent focal seizures generated in the mesio-temporal limbic structures[3, 4]. This period appears as a time of intense functional and morphological reorganization including neurodegeneration, gliosis, axonal damage or sprouting, dendritic plasticity, blood–brain barrier damage, recruitment of inflammatory cells into the brain tissue, reorganisation of the extracellular matrix and of the molecular architecture of individual neuronal cells[5]. To better understand the molecular mechanisms underlying epileptogenesis, microarrays have been used in animal models[6-11] and human samples[12]. Yet, no comprehensive studies at the proteomic level have been performed. Here, we used a mouse model of MTLE induced by intra-hippocampal injection of kainate (KA) which reproduces most of the histopathological and electrophysiological features of human MTLE[13-16]. Indeed, in this model, spontaneous focal epileptic seizures associated with mild behavioral expression develop progressively in the hippocampus, leading to a stereotyped pattern at 16-18 days following KA injection, which remains stable for several months, with only occasional propagation to the cortex, as in MTLE patients[16, 17]. In addition, cell loss in CA1, CA3 and hilus areas, as well as astrocyte proliferation and granule cell dispersion are observed in the kainate-injected hippocampus, that are highly reminiscent of the hippocampal sclerosis

observed in most MTLE patients[13, 14, 18]. In this study animals were sacrificed at specific time-points post KA injection: 1 day post injection (dpi), during the silent period after the completion of the focal *status epilepticus* (SE) when no discharges are observed; 3dpi, during epileptogenesis, when spontaneous seizures start to occur in the hippocampus region, and 30dpi, which corresponds to the chronic phase with recurrent focal discharges.

The employment of label-free strategies for relative protein quantification has gained prominence in the last years due to their ease of use, since no additional sample preparation or chemical modification steps are required[19]. When compared to stable isotope labeling approaches, they provide a simpler method, while also exhibiting a larger dynamic range for estimating relative protein abundance[20].

The most commonly used label-free quantification approach is spectral counting (SC), where relative protein abundance is measured by the number of MS/MS spectra corresponding to all peptides assigned to a protein. Another strategy is based on the sum of the Total Ion Current (TIC) of the MS/MS spectra assigned to the peptides for a given protein[21]. In more recent studies, the intensity of the precursor ion (MS1) is also used as a quantitative measure[22]. SC is easy to use, reproducible and highly sensitive for subtle changes in protein abundance. However, it is considered inaccurate for the calculation of fold change of low abundance proteins, as it is influenced by the protein size[21]. TIC, which is based on the MS/MS spectrum intensity, shows larger dynamic range than SC, improved sensitivity for low abundance changes, but suffers from irreproducibility and signal saturation in highly abundant proteins[19]. Quantification based on precursor ion intensity is considered highly accurate but requires high resolution precursor ion measurements to ensure neighboring peaks are distinguished[23].

Here we employed the combination of all three approaches, in particular (i) SC, (ii) sum of top three TIC values of the peptides of a given protein (top3TIC), and (iii) sum of top three intensities from three precursor ions of a protein (top3 precursor intensity, PI). It has been suggested that top three approaches based on MS1 peak intensity are directly proportional to protein abundance and are associated with fewer errors than SC[24]. Since apparently each of these quantification approaches, which rely on different characteristics of the mass spectra to estimate peptide amounts, has certain advantages and limitations, their combined use should increase the reliability of identified protein changes[21, 23].

The aim of this study was to characterize in detail the temporal protein changes associated with KA-induced MTLE in a mouse model, in order to characterize the disease development at the proteomic level, currently missing in the field, and in parallel provide further experimental evidence for the molecular relevance of this model to human epilepsy. Taken together our results indicate that during epileptogenesis (3dpi) and more importantly during the chronic phase of the syndrome (30dpi), signs of neurodegeneration as well as changes in inflammatory response are observed, possibly through the activation of glial cells and astrocytes.

EXPERIMENTAL PROCEDURES

Animals

Experiments were conducted on adult C57Bl/6j male mice (Janvier, Le-Genest-St-Isle, France; 8-10 weeks of age; 20-25g). After surgery, they were housed in individual cages with food and water *ad libitum* and kept in a 12h light-dark cycle at room temperature (RT). All animal procedures were carried out at the high technology animal platform, Institute Jean Roget (University Grenoble Alpes) and at the Grenoble-Institute for Neuroscience, in accordance with the guidelines of the

European Committee Council Directive 2010/63/EU. All efforts were made to minimize animal suffering and to reduce the number of animals used. The following procedures were approved by the local ethical committee of the University Grenoble Alpes and the Grenoble-Institute for Neuroscience (Protocols #P49, #274).

Intrahippocampal injection

Mice were anesthetized using a mixture of xylazine (4mg/kg, i.p.) and chloral hydrate (400mg/kg, i.p.) and placed in a stereotactic frame in a flat skull position. They were injected with either KA or NaCl (0.9%) as previously described[14-16, 25]. Briefly, a stainless steel cannula (outer diameter, 0.28mm) connected to a 0.5µL micro-syringe (Hamilton, Bonaduz, Switzerland) via PE20 tubing containing distilled water, was filled with a 20mM KA solution (Sigma, Lyon, France) in 0.9% sterile NaCl and positioned in the right dorsal hippocampus (AP = -2, ML = -1.5, DV = -2mm from bregma). Mice received 50nL of the KA solution (1nmol) using a micro-pump (CMA/100, Carnegie Medicin, Stockholm, Sweden). After injection, the cannula was left in place for an additional 1 min to avoid reflux along the cannula track.

After recovery from anesthesia (i.e, about 2h) the animals were observed to visually determine their behavior during the KA-induced SE and confirm impact of the injection. It should be noted that mice were not implanted with electrodes in these experiments to avoid any possible interference on biochemical parameters. However, as published previously[14-16, 25], observations in mice of rotations, postural asymmetry, forelimb clonies and lack of nest building when soft material is provided, during the 24h that follow KA injection, are very robust indicators of the focal status in this model. Based on this phenotypic characterization, no differences in the severity of the phenotype could be observed among the animals. Moreover, KA-injected mice exhibiting recurrent hippocampal paroxysmal discharges, always show astrocytic

proliferation and increased GFAP expression[15, 26]. As described in the results section, for each sample included in the analysis, the overexpression of GFAP was verified by the proteomic analysis, as an "internal" positive control.

Hippocampal dissection

One, three or 30 days after intrahippocampal injection of either KA or NaCl (n=5 mice/group), mice were decapitated. Their brain was rapidly removed from the skull at 4°C. Both the injected and non-injected hippocampi were dissected and the anterior part was snap frozen in liquid nitrogen. The entire procedure never exceeded 2 min. All tissue samples were kept at -80°C until further processed for proteomic analysis.

Proteomic sample preparation

The injected dorsal hippocampi were processed with the filter-aided sample preparation protocol (FASP) (n=5 mice/group)[27]. In more detail, the tissue samples were homogenized in a 0.1M Tris-HCl pH 7 lysis buffer, supplemented with 4% SDS and 0.1M DTT. Following that, protein concentration of the supernatant was determined by Bradford assay and 200μg of protein per sample was mixed with 0.2 mL of 8M urea in 0.1M Tris/HCl, pH 8.5 (urea solution), loaded into 30kDa Amicon Ultra Centrifugal Filters, Ultracel (Merck Millipore) and centrifuged at 14000g for 15 min. The concentrates were diluted in the devices with 0.2mL of urea solution and centrifuged again. After centrifugation, the concentrates were mixed with 0.1mL of 50mM iodoacetamide in urea solution and incubated in the dark, at RT for 20 min (alkylation), followed by centrifugation for 10 min. Then, the concentrate was diluted with 0.1mL of urea solution and concentrated again by centrifugation. The resulting concentrate was diluted with 0.1mL of 50mM NH_4HCO_3, pH 8 and concentrated again by centrifugation. This step was repeated once. Finally, samples were diluted

with 40µL of 25mM NH_4HCO_3 containing 2µg of trypsin. After overnight digestion at RT, peptides were collected by centrifugation of the filter units for 10 min in new tubes. The filter units were washed with another 40µL of 50mM NH_4HCO_3 and remaining peptides were collected in the same tube. The eluates were lyophilized and stored at RT.

LC–MS/MS analysis

The peptide mixtures after lyophilization were resuspended in water (100µl) and were analysed on a Dionex Ultimate 3000 RSLS nano-flow system (Dionex, Camberly UK). 5µl of each sample were loaded onto a Dionex 0.1×20mm 5µm C18 nano trap column at a flowrate of 5µl/min. The loading solution consisted of 98% 0.1% formic acid and 2% acetonitrile. Once loaded onto the trap column the sample was then eluted onto an Acclaim PepMap C18 nano-column 75µm × 50cm, 2µm 100Å at a flowrate of 0.3µl/min. The trap and nano-flow column were maintained at 35°C. The samples were eluted with a gradient of solvent A: 0.1% formic acid verses solvent B: 80% acetonitrile starting at 1% B for 5 min rising to 5% B at 10 min then to 25% B at 360 min then 65% B at 480 min. The column was then washed and re-equilibrated prior to injection of the next sample.

The eluate from the column was applied to a Proxeon nano-spray ESI source (Thermo Fisher Hemel UK) operating in positive ion mode into an Orbitrap Velos FTMS (Thermo Finnigan, Bremen, Germany). Ionization voltage was 2.6kV and the capillary temperature was 200°C. The mass spectrometer was operated in MS/MS mode scanning from 380 to 2000amu. The top 20 multiply charged ions were selected from each scan for MS/MS analysis and the fragmentation method was CID at 35% collision energy. The resolution of ions in MS1 was 60,000 and 7,500 for CID MS2 which was performed in the Orbitrap. The data was acquired using data dependent

settings with dynamic exclusion enabled, a repeat count of 1 with exclusion duration of 15 seconds. The threshold for triggering a MS/MS event was set at 10,000 counts and the isolation width of precursor ion was 2, charge state screening was enabled and unassigned charge states and a charge state of 1 were rejected.

LC–MS/MS -data processing

Tandem mass spectra from LC–MS/MS analysis of the samples were uploaded to Thermo Proteome Discoverer 1.4 software (Thermo Scientific, Hemel Hempstead, UK). Precursor peptide mass tolerance was set at 10ppm and 0.4Da for MS/MS fragment ions. Peptide and protein identification was performed with the SEQUEST search engine. For peptide identification the latest version of the UniProt SwissProt database of *Mus musculus* proteome containing only reviewed canonical sequences (17046 entries, 29/10/2014) was used, considering trypsin enzyme digestion and allowing for a maximum of one missed cleavage. Carbamidomethylation of cysteine was specified as a fixed modification and deamidation of asparagine and glutamine and oxidation of methionine were specified as variable modifications in SEQUEST. All acquired information regarding the identified proteins, including score, sequence coverage, number of assigned peptides, protein area, as well as peptide sequences and areas, are provided in Supplementary Table 1.

Scaffold (version Scaffold_3.6.3, Proteome Software Inc., Portland, OR) software was used to validate MS/MS based peptide and protein identifications at each time-point. Peptide and protein identifications were accepted if they could be established at greater than 90.0% and 99.0% probability, respectively, by the Peptide Prophet and Protein Prophet algorithm[28, 29]. Proteins that contained similar peptides and could not be differentiated solely based on MS/MS analysis were grouped to satisfy the principles of parsimony. Using a target decoy database, a peptide false discovery rate

lower than 0.05% was determined. Protein identifications were accepted if they included at least 2 identified peptides in at least one biological sample.

Label-free quantification of protein expression levels in the resulting hits was performed in Scaffold, using 3 different quantification approaches: Spectral counting (SC), the sum of the top three TIC values of the peptides of a given protein, and the sum of the top three intensities from three unique peptides (MS1 intensity) of a protein (Precursor intensity, PI). SC corresponds to the "sum of all unweighted spectrum counts of each MS samples". TIC is the "sum of the areas under all the peaks contained in a MS/MS spectrum. Scaffold assumes that the area under a peak is proportional to the height of the peak and approximates the TIC value by summing the intensity of the peaks contained in the peak list associated to a MS/MS sample". Data were normalized by Scaffold. Following that, fold expression difference was calculated in KA-injected mice versus NaCl-injected mice at each time-point and statistical analysis was performed with the Student's *t*-test (Supplementary Table 1).

Immunohistochemistry

All animals were perfused transcardially with 4% paraformaldehyde in phosphate buffer saline (PBS) (n=4 mice/group). Brains were cryoprotected in 20% sucrose in PBS, embedded in cryomedia (OCT), sectioned (40µm) with a cryostat in coronal orientation and were further processed for immunohistochemistry assays. Free-floating sections were pre-incubated in 0.25% Triton X-100 in PBS for 30 minutes at RT and then in PBS containing 2% bovine serum albumin (BSA, blocking solution) as a blocking agent for 30 minutes at RT. Next, sections were incubated overnight in BSA containing 0.1% Triton X-100 and the primary antibody at 4˚C. After rinsing four times with PBS, sections were incubated for 2h at RT with fluorescence-conjugated secondary antibody diluted in PBS. Following that, nuclei were stained

with Hoechst dye, diluted 1:1000 in PBS. Finally, sections were rinsed 4 times in PBS and mounted on slides. Microscopic images were obtained using a Zeiss confocal microscope.

Multiple reaction monitoring LC-MS/MS - Sample Preparation

Peptides corresponding to 100µg total protein tissue extract from the FASP preparation were used for Multiple reaction monitoring (MRM) LC-MS/MS analysis (30dpi; n=5/group). The peptide mix was desalted with Zip-tips (Thermo Scientific), dried using a vacuum centrifuge and pellets were solubilized in appropriate volume of 0.1% formic acid (FA) to 1µg/µL final concentration.

MRM LC-MS/MS assay design and method development

Liquid chromatography was performed using an Agilent 1200 series nano-pump system (Agilent Technologies, Inc., Palo Alto, CA), coupled with a C18 nano-column (150mm × 75µm, particle size 3.5µm) from Agilent. Peptide separation and elution was achieved with a 40 min 5-35% ACN/water 0.1% FA gradient at a flow rate of 300nl/min. Four microliters of each sample were injected.

Tryptic peptides were analyzed on an AB/MDS Sciex 4000 QTRAP with a nano-electrospray ionization source controlled by Analyst 1.5 software (Sciex). The mass spectrometer was operated in MRM mode, with the first (Q1) and third quadrupole (Q3) at 0.7 unit mass resolution. At least three transitions were recorded for each peptide. Optimum collision energies for each transition were automatically calculated by the Skyline software. Detailed information about the acquisition method and the used parameters are provided in Supplementary Table 2 (supporting information document).

Proteotypic peptide selection for MRM LC-MS/MS

Proteotypic peptides for GFAP, Apolipoprotein-E, Clusterin, Vimentin, Cystatin-C, Galectin-1, Gelsolin, and Homer 1 were selected from the list of proteotypic peptides provided by Skyline[30]. The final selection was based on the quality of the MS/MS spectrum of each peptide in the mouse spectral library (NIST_mouse_IT_2012-04-21_7AA.splib), downloaded from NIST (National Institute of Standards and Technology, http://www.nist.gov/), and on the score and number of observations in MS-based proteomics experiments as provided from PeptideAtlas (www.peptideatlas.com)[31]. One up to three proteotypic peptides with at least 3 transitions each, were finally selected to be tested.

RESULTS

Intrahippocampal kainate injection induces initial status epilepticus and GFAP upregulation

As extensively described in previous studies, a single dose of KA (1nmol in 50nl) induced an initially focal status epilepticus lasting up to 15-20h, during which animals showed mild asymmetric clonic movements of the forelimbs, rotations, and/or behavioral arrests[13-18]. Following KA administration, all mice evaluated in this study had behavioral signs of SE on day 0. Then, they progressively displayed 15-20 sec duration focal seizures associated with behavioral arrest, chewing and head nodding during the first 2-3 weeks[14, 16]. As described earlier (methods), mice were not implanted with electrodes in these experiments. Efficiency of injection was instead monitored by observing specific phenotypic and behavioral characteristics during the 24h that follow KA injection (rotations, postural asymmetry, forelimb clonies and lack of nest building when soft material is provided). Based on these characteristics,

no differences in the severity of the phenotype could be observed among the animals. In addition, activation of astrocytes and reactive astrogliosis has been reported as a hallmark of neuronal loss in neurodegenerative disorders and epilepsy[32-34]. Previous studies have established that KA-injected mice exhibiting recurrent hippocampal paroxysmal discharges always show astrocytic proliferation and increased GFAP expression[15, 25]. GFAP is therefore considered as a positive control, reflecting the efficiency of the KA injection and focal status[25, 35]. As shown in Figure 1A, all mice included in the study exhibited an increase of GFAP expression after KA injection in comparison to NaCl treated mice according to the proteomics analysis (at 3dpi $\geq$1.5 fold and at 30dpi $\geq$9 fold, $p<0.05$, Student's t-test). GFAP upregulation was further confirmed by immunohistochemistry, showing a gradual increase of 1.6, 2 and 3.9 fold at 1dpi, 3dpi and 30dpi respectively, in comparison to NaCl treated mice (Figure 1 B, C, n=4/group).

Label-free quantitative proteomic analysis

Global protein analysis of KA and NaCl-injected hippocampi of three distinct time-points by LC-MS/MS resulted in the detection of a total of 1309 proteins at 1dpi, 1481 at 3dpi and 1280 at 30dpi, respectively (Figure 2, Supplementary Table 1**)**. Low percentage of variance (Coefficient of variance of less than 21%) in number of identified proteins was detected among the different biological replicates per time-point (Supplementary Figure 1). Good reproducibility rates were observed in all cases with 83.5% and 90.5% of proteins identified in at least 3 out of 5 replicates in KA and NaCl treated mice at 1dpi, respectively. The respective rates for 3 and 30dpi were 85.2% (KA) and 87.8% (NaCl) at 3dpi, and 90% (KA) and 83.5% (NaCl) at 30dpi (Supplementary Figure 2). To increase reliability of findings a frequency threshold was applied and only proteins present in at least 3 out of 5 samples in both groups

(KA and NaCl) or uniquely expressed in at least 3 out of 5 KA or NaCl treated mice, were considered for further differential expression analysis (Figure 2).

For the label-free quantification of protein expression changes, three quantification approaches were applied in Scaffold software: SC, top three TIC and top three PI. Following comparison of KA vs NaCl-injected mice at each time-point and statistical analysis, proteins that were differentially expressed (fold change≥1.5 or fold≤0.5) and statistically significant ($p \leq 0.05$, Student's *t*-test), in at least one quantification approach, were in total 183 (1dpi), 187 (3dpi) and 363 (30dpi) (Supplementary Figure 3). However, at 1dpi, only 9 proteins were overlapping among the three approaches, which corresponds to a range of 8-16% overlap, depending on the performed comparison [Supplementary figure 3, A(i)]. Higher overlap was observed at 3 and 30dpi, with 20-27% and 36-40% overlap among the three quantification approaches, respectively [Supplementary figure 3, B(i), C(i)]. Of note, the overlapping proteins of all three approaches are not always the ones with the lowest p values. In particular, among the top 20 or top 50 of the proteins with the lowest p values per quantification approach, only 15-26% proteins were overlapping among all 3 approaches, at each time-point (data not shown).

Overlap was also investigated considering one of the two criteria being fulfilled (e.g. either $p \leq 0.05$ or fold change≥1.5/fold ≤0.5 but with agreement in expression trends). Data show similar overlap when all proteins with $p \leq 0.05$ are taken into account [1dpi (7.5-14.3%), 3dpi (22.5-29%), 30dpi (38.5-42.5%), Supplementary figure 3 A(ii), B(ii), C(ii)], while overlap increases to 40-50% when only the fold change threshold is used [1dpi (39.6-56.9%), 3dpi (43.6-48.4%), 30dpi (41-56.7%), Supplementary Figure 3 A(iii), B(iii), C(iii)]. Taken together, these data indicate a low number of overlapping proteins when the statistical significance in taken into account. We

nevertheless decided to consider for further analysis differentially expressed proteins as defined by fold change (fold≥1.5 or fold ≤0.5) and statistical significance ($p \leq 0.05$, Student's t-test), as well as proteins uniquely expressed in at least 3 out of 5 KA or NaCl treated mice, according to all 3 quantification approaches. Even though this approach apparently decreases the number of shortlisted proteins for further investigation, it increases confidence and reliability of highlighted findings, which is important considering the relatively small sample size (n=5/group) and general trend of such multi-parametric omics analyses towards providing false associations. According to these criteria, the highest number of differentially expressed proteins was observed at 30dpi (175 proteins), whereas 22 proteins were differentially expressed at 1dpi and 53 proteins at 3dpi (Figure 2, Supplementary Table 1).

Immediate protein expression response after SE (1dpi)

Proteomic analysis revealed that, following KA administration, mice that had developed SE showed a small number of proteins being regulated, 1 day post KA injection. In particular, twenty-two proteins were found to be differentially expressed (Table 1). Interestingly, most of the differentially expressed proteins at 1dpi were downregulated in KA-injected mice or expressed only in control animals (NaCl-injected mice). Well-known proteins involved in synaptic plasticity, such as Neurabin-2 and Neurochondrin, or involved in neurodegeneration such as Homer1 were downregulated by 0.66, 0.33 and 0.53 fold, respectively[36-38]. Additionally, other proteins expressed in neuronal cells were detected only in NaCl-injected animals, such as Ataxin-10, Shank3 and WD repeat-containing protein 47[39-41]. On the other hand, some proteins that have also been shown to be expressed by neural cells were upregulated, such as nucleophosmin (2 fold), or detected only in KA-injected animals such as SPARC-like protein 1 and Hemopexin[42-44].

Early protein expression response during epileptogenesis (3dpi)

The proteomic data at 3dpi depicted 53 proteins which were significantly changed following KA administration, and in particular 21 proteins were upregulated or detected only in KA-injected mice, whereas 32 proteins were downregulated or detected only in control (NaCl-injected) animals (Supplementary Table 1). As shown in Figure 3A, and following grouping based on gene ontology (using Panther[45]), at 3dpi several differentially expressed proteins following KA injection were associated to neuron projection development and regulation of synaptic plasticity, as well as microglial cell and astrocyte activation (Table 2). In brief, most of these proteins, such as Neurabin-2, Brain-specific angiogenesis inhibitor 1-associated protein 2, Src substrate cortactin, Sodium- and chloride-dependent GABA transporter 1 were downregulated 0.3, 0.36, 0.47 and 0.53 fold, respectively. Similarly, other molecules involved in neuronal synaptic processes, such Brain-specific serine/threonine-protein kinase 1, A-kinase anchor protein 5 and Shank3 (SH3 and multiple ankyrin repeat domains protein 3) were detected only in NaCl-injected mice. By contrast, proteins found to be significantly upregulated at 3dpi, were indicative of glial and astrocyte cell differentiation as well as lymhpocyte migration. These include Moesin (8.3 fold), Clusterin (2.73 fold), GFAP (1.9 fold) and Vimentin (2 fold) (Table 2).

Protein expression response during chronic phase of epilepsy (30dpi)

In the hippocampi collected at 30dpi, i.e., during the chronic phase of epilepsy, 175 proteins were found to be differentially expressed, in comparison to NaCl-injected animals. In particular, 97 proteins were found to be upregulated or detected only in KA-injected mice, whereas, 78 proteins were detected as downregulated in KA-injected mice or detected only in control animals (Supplementary Table 1). A significant number of the dysregulated proteins were related to neuron and axon

regeneration, regulation of synaptic plasticity, inflammatory response, microglial cell activation, using grouping based on gene ontology (Panther[45]), (Figure 3 B, C). All proteins related to these categories are listed in Table 3. Similar results regarding the GO terms enriched in the differentially expressed proteins were also obtained following data analysis using Cytoscape software[46] (data not shown). In addition and in support of the specificity of this finding, when Panther analysis was performed using 3 randomly picked similar sized protein datasets or the whole dataset of non-differentially expressed proteins, in general a lower enrichment of GO terms related to neuronal processes or immune response was obtained in comparison to the respective analysis of differentially expressed proteins (e.g. at 30dpi terms related to neuronal processes showed an enrichment of 2.29-10.86% in the differentially expressed proteins in comparison to 1.1-4.1% and 2-5.58% enrichment in randomly picked similar sized protein dataset or in the whole dataset of non- differentially expressed proteins, respectively).

The vast majority of proteins related to neuronal responses were downregulated or detected only in NaCl-injected animals, which could be an indication of neurodegeneration induced in the KA-injected animals. These included Src substrate cortactin (0.13 fold), Drebrin-like protein (0.2 fold), Paralemmin-1 (0.2 fold), Band 4.1-like protein 3 (0.26 fold), Disks large homolog 2 (Dlg2) (0.23 fold), Disks large homolog 4 (Dlg4) (0.3 fold) and Map1b (0.43 fold), all significantly down-regulated. In addition, some proteins found to be down-regulated at 3dpi appeared consistently also down-regulated at 30 days post KA injection, as shown in Table 4. These included: Brain-specific angiogenesis inhibitor 1-associated protein 2 (3dpi: 0.37 fold, 30dpi: 0.16 fold), Neurabin-2 (3dpi: 0.3 fold, 30dpi: 0.4 fold), Map1a (3dpi: 0.6 fold, 30dpi: 0.43 fold), Map2 (1dpi: 0.53 fold, 3dpi: 0.53 fold, 30dpi: 0.43 fold) and

Sodium- and chloride-dependent GABA transporter 1 (3dpi: 0.53 fold, 30dpi: 0.37 fold). Table 4 highlights all proteins which are differentially expressed in more than one time-point. Interestingly, these markers show consistent upregulation or downregulation during the progression of the epileptic syndrome.

Moreover, several 14-3-3 proteins commonly expressed in the brain were downregulated, including beta/alpha (0.59 fold), gamma (0.63 fold), epsilon (0.66 fold), eta (0.59 fold), theta (0.59 fold).

At the same time-point, consistent upregulation of proteins related to inflammation and immune response as well as astrocyte and glial cell activation was observed following KA injection, in comparison to controls (Figure 3C, Table 3, Table 4). In particular, several proteins mainly expressed by activated glial cells and astrocytes were upregulated, such as Clusterin (37.5 fold), GFAP (12.5 fold), Vimentin (8 fold), Gelsolin (6.4 fold), Apolipoprotein E (5.2 fold) and Allograft inflammatory factor 1 (Iba-1) (detected only in KA-injected mice). Additionally, proteins indicative of inflammation and immune response were also found to be mostly upregulated or detected only in KA-injected animals, including Cystatin-C (4.1 fold), Alpha-2-macroglobulin, Complement C4-B, Galectin-1, CD44 antigen and Platelet-activating factor acetyl hydrolase, all detected only in KA mice.

Targeted proteomic MRM LC-MS/MS

From the differentially expressed proteins at 30dpi, several molecules which are predominantly expressed by astrocytes and microglia such as GFAP, Vimentin, Clusterin, Apolipoprotein E and Gelsolin, as well as molecules that are abundantly present in inflammation sites such as Cystatin-C and Galectin-1, were selected for validation with an MRM targeted proteomic approach. Selection of these proteins for further validation was based on biological relevance (e.g. involvement in activation of

microglia and inflammation), as well as ability to develop MRM assays for their measurement (availability of proteotypic peptides of good chromatographic and mass spectrometric properties). MRM LC-MS/MS analysis confirmed the upregulation of all these molecules upon KA injection (Figure 4, Table 5, Supporting information-Table 3). As shown, GFAP and Apolipoprotein E were detected with three and two peptides, respectively, all following the same trend of expression. In these experiments, Homer 1, which was detected by LC-MS/MS in both KA and NaCl-injected animals at equal levels at 30dpi, was used as a control. Indeed, Homer 1 was also found to be equally expressed in KA and NaCl-injected hippocampi by MRM LC-MS/MS.

DISCUSSION

In the present study, we provide an overview of the temporal proteomic regulation that takes place during development of epilepsy, in a well-defined model of MTLE[16, 25]. For this reason, distinct time-points after KA injection were selected for further analysis. The first time-point, 1 day post injection, is during the silent period, right after the initial seizure, when no discharges are observed upon completion of the focal status epilepticus. The second time-point, 3 days post injection, is when epilepsy develops (epileptogenesis), and spontaneous seizures start to occur in the hippocampus region; whereas the 30dpi time-point, corresponds to the chronic phase of epilepsy with recurrent stereotyped focal discharges[47]. This model of intra-hippocampal KA injection has been well characterized in many studies as successfully reproducing most of histopathological and electrophysiological features of human MTLE[13-16]. Yet, the proteomic profile associated with these gross phenotypic changes has not been studied. Our study based on application of label-free LC-MS/MS analysis in combination to relative quantification using 3 different

strategies, provides the first underlying proteomic changes giving rise to the observed phenotype. Specifically our analysis clearly demonstrates downregulation of molecules related to neuron/axon regeneration and synaptic plasticity, also indicating neurodegeneration especially during the chronic phase of the syndrome. In parallel, activation of microglial cells and regulation of inflammation is predicted even at the 3dpi time-point, suggesting astroglial mediated inflammatory response initiating early and persisting during the chronic phase of epilepsy.

Combination of three label-free quantification approaches

Label-free quantification strategies have been widely utilized in shotgun proteomic analyses due to their ease of use in detecting differences in protein abundance in biological samples. In this study, we employed a combination of three such quantification approaches, SC, top three TIC and top three PI, each one based on a different feature of the LC-MS/MS data analysis for protein quantification. In particular, these approaches which are based on Spectral count, MS/MS intensity and MS1 intensity, respectively, have been shown to have certain advantages and limitations (also described in the introduction section). In brief, SC has been considered as a more sensitive approach in detecting proteins that undergo changes in abundance, in comparison to intensity based approaches[23]. MS/MS TIC has been shown to improve sensitivity in detection of relative changes in low abundant proteins, in comparison to SC[21]. On the other hand, peak area intensity measurements are considered to have better performance than MS2-based approaches, regarding reproducibility and quantitative dynamic range[48]. More interestingly, it has been suggested that SC-based protein abundance measurements are comparable to intensity-based approaches (PI) with respect to correlation with gene expression data[49]. Based on the presented data, we believe that no solid conclusions may be

drawn with respect to superiority of one approach versus the others. Similar proteins in terms of GO annotations were found to be enriched by all approaches (data not shown), and there is general agreement in the expression trends among overlapping proteins (Supplementary Table 1). The added value of using all 3 approaches is mainly in prioritizing and shortlisting differentially expressed proteins, in such a multi-parametric (high number of variables, low n) quantification approach, hence increasing reliability of presented conclusions.

Deregulation of a limited number of immediate response proteins

Following KA administration, a small number of immediate early response proteins were regulated, as depicted by protein expression changes at 1dpi. Proteins interacting with or regulating glutamate receptors and involved in neuronal plasticity were found to be down-regulated in KA- versus NaCl- injected mice: these include Neurochondrin (Ncdn[36]; down-regulated by 0.66 fold), Homer1[38] (down-regulated by 0.53 fold) and Shank 3 (SH3 and multiple ankyrin repeat domains protein 3; detected only in NaCl-injected mice at 1dpi and earlier shown to interact with Homer 1[40]). According to recent studies, Homer 1 is increased in hippocampus right after status epilepticus in another model of TLE[50], but downregulated in microarray analysis of human TLE samples[51], in line to our studies. Similarly, Ataxin-10 was also detected only in NaCl-injected mice; this protein is widely expressed in the brain and has been involved in induction of neuritogenesis[39]. Neurabin-2 (Spinophilin), a scaffolding protein of neuronal dendritic spines that regulates synaptic transmission[37] was downregulated at 1dpi in KA-injected mice (0.33 fold). On the other hand, one of the upregulated proteins, nucleophosmin (2 fold), regulates key cellular processes, directly linked to proliferation[42, 52]. Recently it was suggested that nucleophosmin, in the case of insult, may act as a coordinator of a response that can lead to cell death[42].

Altogether, these data suggest that impairment of synaptic plasticity is already evident during the so-called "silent period" that follows status epilepticus.

Downregulation of neuronal related proteins is indicative of neurodegeneration

TLE is characterized pathologically by hippocampal sclerosis, a characteristic morphologic change associated with massive hippocampal neuronal loss localized in the hilus of the dentate gyrus, as well as in the CA1 and CA3 hippocampal regions[53]. Similar histopathological features are observed in the KA treated mouse model of MTLE[13-16]. Proteomic analysis revealed that during epileptogenesis, i.e. at 3dpi, several molecules related to neuron projection, axon and dendrite development as well as synaptic plasticity and transmission were downregulated. Most of these proteins were also found to be downregulated at 30dpi, suggesting a sustaining phenomenon of neurodegeneration (Table 4). More specifically, Brain-specific angiogenesis inhibitor 1-associated protein 2, an abundant component of the postsynaptic density, shown to interact with Rac and ProSAP/Shank proteins and considered a regulator of hippocampal synaptic plasticity[54, 55] as well as Brain-specific serine/threonine-protein kinase 1, a presynaptic regulator of neurotransmitter release[56], were significantly downregulated (0.37 fold, 3dpi; 0.16 fold, 30dpi) or detected only in NaCl-injected animals at 3dpi, respectively. Shank3, which interacts with metabotropic glutamate receptors, was again detected only in NaCl-injected animals at 3dpi, as in the case of 1dpi. Molecules involved in synaptic transmission, such as Neurabin-2, (also involved in antigen presentation of dendritic cells)[37], and A-kinase anchor protein 5 (Akap5), a postsynaptic scaffold molecule involved in long term potentiation[57], were consistently downregulated [0.33 (1dpi), 0.3 (3dpi), 0.4 (30dpi)] in KA-injected animals or detected only in NaCl animals (3dpi, 30dpi), respectively. Another molecule that seems to be involved in regulation of neuronal spine density is Src substrate cortactin

(Cttn), which was also found to be downregulated in KA-injected mice at 1dpi (0.53 fold), 3dpi (0.47 fold) and at 30dpi (0.13 fold)[58]. Neuron specific microtubule-associated proteins Map1a, Map2, tau (Mapt), Map1b and Map6, participating in the development of neuronal polarity[59-64] were found to be down-regulated: Map2 consistently downregulated in all three time-points after KA injection [by 0.53 (1dpi), 0.53 (3dpi) and 0.43 (30dpi)], Map1a at 3 and 30dpi [0.6 (3dpi), 0.43 (30dpi)] and tau, Map1b and Map6 at 30dpi (tau: 0.37, Map1b: 0.43 and Map6: 0.3 fold). Drebrin-like protein (Abp1), which plays an important role on synaptic organization and neuron morphogenesis[65], was significantly downregulated (0.2 fold) at KA-injected mice at 30dpi. Paralemmin-1, which is required for dendritic spine maturation through filopodia induction, was also downregulated in KA-injected animals 30dpi (0.2 fold)[66].

Interestingly, many molecules related to glutamate signaling and GABA synthesis, such as Disks large homolog 4 (PSD-95), Disks large homolog 2 (PSD-93) that interact with NMDA receptors and Band 4.1-like protein 3 that interacts with AMPA receptors, were downregulated by 0.3, 0.23 and 0.43 fold respectively, in KA-injected mice at 30dpi. This later result could be expected since KA is an agonist of the kainate receptors[14, 67] and is in line with our recent report in the same model showing a reduced expression of several subunits of NMDA and AMPA receptor (Stamboulian et al, under submission). However, further studies are still needed to clarify the involvement of these proteins of the glutamate receptor signaling pathway to the development of the epileptic phenotype in the KA model. Moreover, expression of Protein kinase C gamma type (PKC gamma), which binds to GLUR4 and NMDAR1 neuronal receptors and plays a key role in neuronal signal transduction as well as in protection from oxidative stress[68, 69] was also downregulated in KA-injected mice at

30dpi (0.59 fold). Taken together these findings further confirm and provide the molecular background of the established phenotype of neurodegeneration observed in the KA mouse model.

Consistent upregulation of proteins related to microglia/astrocyte activation and inflammatory response

Inflammation in the brain and the rest of the central nervous system (CNS) is a key factor in development of neurodegeneration[60]. Although the CNS has been considered to be immunologically privileged, as peripheral circulating immune cells have only limited access to it, dynamic immune and inflammatory processes occur in response to different stimuli[60]. Microglia is a first line of defense in response to CNS injuries or immunologic stimuli. It is activated, undergoes phagocytosis, antigen presentation, proliferation and releases inflammatory mediators, such as cytokines, chemokines, nitric oxide and ROS[61]. Although the initial neuroinflammation is protective for the CNS, in specific pathological conditions, it can persist long after an initial insult. This inflammatory response mobilizes other cells like astrocytes, T cells and even neurons, which participate in a self-perpetuating neurotoxic phenomenon[61]. In MTLE many alterations in the intermediate and chronic phase after injury, such as abnormal migration of neurons, aberrant synaptic reorganization, greatly declined neurogenesis and sustained inflammation, have been reported[25]. In brain tissue from epileptic patients, astrocytes undergo significant changes in their physiological properties, and are involved in the activation of inflammatory pathways[70]. In particular, reactive astrogliosis with modified astroglial function may play an important role in the generation and spread of seizure activity[71]. It has been suggested that proinflammatory molecules can change glio-neuronal communications and contribute to the generation of seizures and seizure-related neuronal damage[70].

In the KA MTLE mouse model, our data obtained at 30dpi show that proteins mainly expressed by astrocytes and microglia were upregulated or expressed only in epileptic mice, suggesting glial cell activation and/or astrocyte differentiation. Some of these proteins were already significantly upregulated at 3dpi (Table 4), suggesting that this effect on astrocytes is initiated during epileptogenesis, in line with previous findings[25]. At the same time-point a significant number of molecules related to inflammation and immune response was upregulated, also in support of an astrocyte/microglial-mediated inflammatory response.

In particular, GFAP and Vimentin, markers of astrocyte and radial glial cells, respectively[35, 72-74] were found to be upregulated at 3dpi (GFAP: 1.9 fold; Vimentin: 2.1 fold), and 30dpi (GFAP: 12.5 fold; Vimentin: 8 fold). Along the same lines, Clusterin (Sulfated glycoprotein 2, SGP-2, or apolipoprotein J), predominantly expressed in astrocytes and suggested to be neuroprotective in neurodegenerative diseases[75] ,was upregulated at 3dpi in KA-injected mice (2.5 fold) and even more at 30 dpi (37.5 fold). Along the same lines, Apolipoprotein E (ApoE), main apolipoprotein expressed by astrocytes and potential modulator of inflammation[76, 77]. and Gelsolin, mainly expressed by activated microglia and astrocytes[78] and with potential protective role against neuroinflammation in the brain[79], were also upregulated in KA-injected mice (5.2 fold and 6.4 fold respectively) at 30dpi. Additional astrocyte or microglial markers found to be upregulated at 30dpi include, Aldehyde dehydrogenase 1 family, member L1 (Aldh1L1)[80], as well as Allograft inflammatory factor 1 (Iba-1)[81], collectively all suggesting significant glial activation at the chronic phase of MTLE.

In support of this hypothesis, a significant number of molecules related to inflammation and immune response were also found to be upregulated in KA vs

NaCl-injected animals, at 30dpi. Specifically, it has been suggested that activation of microglia induces the release of proinflammatory cytokines as well as complement components[82]. Along these lines, serum acute phase proteins produced upon tissue inflammation, such as complement C4B and the inflammatory marker alpha-2-macroglobulin[83] were detected only in KA-injected mice at 30dpi. In addition, Galectin-1, earlier reported to be abundantly present at inflammation and injury sites, and also shown to be upregulated in degenerating neurons[84, 85] was detected only in KA-injected mice. Along the same lines, Cystatin-c, earlier reported to be upregulated during chronic epilepsy, implicated with decreased neurogenesis and recently been considered as marker of inflammation[86], was significantly upregulated in KA-injected mice at 30dpi (4.1 fold). Additional molecules related to immune responses and found to be expressed only in KA-injected animals at 30dpi included CD44[87], two integrin receptors, Integrin alpha-V (CD51) and Integrin beta-2 (CD18) expressed by T cells[88], and Platelet-activating factor acetylhydrolase, a molecule with potent pro-inflammatory properties[89].

Taken together, these findings suggest that signs of neuroinflammation, likely mediated through astrocyte and microglia activation, in the hippocampus of MTLE mice are evident at 3dpi, during epileptogenesis, and persist during the chronic phase of epilepsy up to 30dpi.

Validation of findings in other studies of human/mouse MTLE samples

The KA mouse model used in this study is a well-established model of MTLE. It reproduces most of the behavioral, electrophysiological, histological and pharmacological features observed in human patients suffering of MTLE, as depicted by clinical epileptologists[47, 90, 91]. A large number of publications have used this model including recent investigations on the most commonly used antiepileptic drugs[13-16, 47].

Nevertheless, similarities of the mouse model to the human condition at the molecular level have not been investigated, as to the best of our knowledge there is not enough human data yet to allow such quantification of molecular similarities. As a first effort in this direction, we crosschecked our proteomic findings in existing studies of human MTLE samples. As mentioned previously, at 30dpi mice have regular and stable focal seizures with no further evolution, thereby this time-point is considered to correspond to the chronic state of the disease, hence be reflective of the observed human condition[16, 47]. As we can see in detail in Table 6, mouse data from 30dpi are in very good agreement with genomic or proteomic data from human MTLE samples, validating the increased relevance of this model to human MTLE[91]. Even though such analysis to be completed further requires a more detailed cross-species evaluation of orthologues, various interesting observations can already be made: Our data are in good agreement with DNA microarray data analyzing the gene expression profile of sclerotic hippocampi surgically removed from TLE patients[51]. In particular, GFAP, GMP reductase, Moesin and CD44 were upregulated, whereas DLG4, Homer 1, Synapsin-1, MAP2K4 and PTK2B (FAK2) were downregulated according to the microarray analysis[51], in line to our proteomics results. Interestingly, GFAP Moesin MAP2K4, PTK2B and Homer1 were detected as being differentially expressed, from a very early time-point (3dpi) in the mouse model. Their further investigation as potential early markers for the human syndrome is warranted. In other microarray studies of human MTLE samples, Serotransferrin and Tenancin were upregulated while Amphiphysin was downregulated, in good accordance with our data[12, 92, 93]. When proteomic analysis using two-dimensional gel electrophoresis (2-DE) coupled with mass spectrometry was performed in human MTLE hippocampi, differential

expression of Ezrin (up, 5.3 fold) and Map2k4 (down, 0.56 fold) was suggested, in agreement with our findings[94].

Besides the relevance to the human pathology, additional proteomic changes reported in our study were also observed in other studies using the KA mouse model of MTLE, mainly by immunohistochemistry. Specifically, elevated expression of the astocyte marker GFAP was validated at several time-points, 3dpi, 7dpi, 14dpi and 6 weeks post KA injection[15, 25] (Table 6). Moreover, upregulation of the microglial marker Iba-1 has also been verified in KA-injected animals at 7dpi[15] and 14dpi [95].

Uncovering the underlying molecular mechanisms involved in MTLE is critical to obtain a better understanding of the pathophysiology of epileptogenesis. Our study, relying on the use of robust proteomic approaches in combination to targeted MRM analysis, provides a comprehensive molecular background associated with deregulation of neuronal processes even at 1dpi, followed by activation of microglia, induced inflammation and neurodegeneration during epileptogenesis, sustained and significantly expanded at the chronic phase of the epilepsy. Even though further studies are needed to confirm the biological relevance of these findings, their agreement in several cases with those of available studies using human samples, further enhances the applicability of this model in drug development and forms the basis for new studies addressing the upstream regulators of the observed astroglial inflammatory response.

FIGURE LEGENDS

Figure 1

Time course of GFAP expression in the dentate gyrus after unilateral intrahippocampal KA injection. (A) All mice included in the study exhibited an increase of GFAP expression as shown by the proteomics analysis. Upregulation by 1.3 (not reaching statistical significance), 1.9 and 12.5 fold, (average of the three quantification approaches), was detected at 1dpi, 3dpi and 30dpi, respectively (n=5/group). Data from spectral counts are presented, similar results were obtained from all approaches. (B) Confocal images showing double immunostaining for GFAP (green) and Hoechst (blue) on ipsilateral sections of the dentate gyrus at 1dpi (i), 3dpi (ii) and 30dpi (iii), (n=4/group). (i-iii) GFAP gradual upregulation in the dentate gyrus is shown, reaching maximum levels at 30dpi. Hoechst staining shows dispersion of the dentate gyrus especially at 30 d post KA injection. (iv) Minimum GFAP expression levels were detected on ipsilateral sections of the dentate gyrus of control NaCl-injected mice; representative image at 30dpi is shown. Magnification 20x. (C) Semi-quantitative analysis of GFAP expression based on the immunohistochemistry images. Gradual increase of 1.6, 2 and 3.9 fold is observed at 1dpi, 3dpi and 30dpi, respectively, in comparison to NaCl controls (n=4/group, Student's *t*-test). The number of GFAP positive cells per 100mm^2 is depicted (ImageJ software).

Figure 2

Overview of the proteomic findings of KA vs NaCl-injected animals, at 1, 3 and 30dpi. Average number of proteins identified per sample using Scaffold software, with a peptide FDR<0.05% and at least 2 identified peptides per protein are shown. Collected protein lists of all samples (n=5/group) per time-point were merged and

then a frequency threshold was applied, as follows. Only proteins present in at least 3 out of 5 samples or uniquely expressed in at least 3 out of 5 KA or NaCl treated mice, were considered for further analysis. Following comparison of KA vs NaCl-injected mice at each time-point and statistical analysis, proteins that were differentially expressed (fold change≥1.5 or fold≤0.5) and the differential expression was statistically significant ($p \leq 0.05$, Student's *t*-test), according to all 3 quantification approaches (SC, top three TIC and top three PI), were shortlisted.

Figure 3

Functional annotation of differentially expressed proteins. Functional annotation of the differentially expressed proteins at 3dpi (A) and 30dpi (B, C) using Gene Ontology (biological process), revealed that a number of proteins were related to neuron projection, axon and dendrite development, synaptic plasticity as well as microglial and astrocyte activation.

Figure 4

Validation of selected findings using MRM LC-MS/MS. Representative box plots of the intensity of specific proteotypic peptides used for the identification/quantification of GFAP, Vimentin and Apolipoprotein-E in KA and NaCl treated animals, are shown. A total of 5 samples per category were analyzed.

TABLES

Table 1

1dpi – All differentially expressed proteins

1dpi: Following comparison of KA vs NaCl-injected mice and statistical analysis (Student *t*-test), proteins that were differentially expressed (fold change≥1.5 or fold ≤0.5) and the differential expression was statistically significant ($p \leq 0.05$, Student's *t*-

test), according to all 3 quantification approaches (SC, top three TIC and top three PI), are shown. Only proteins present in at least 3 out of 5 samples or uniquely expressed in at least 3 out of 5 KA or NaCl treated mice, were included. Average of the fold change (KA/NaCl) of each quantification approach is shown. Detailed information on mean intensities of all proteins and p values for each quantification approach are shown in Supplementary Table 1.

Table 1: 1dpi – All differentially expressed proteins

Entry name	Protein name	Gene name	Fold change
TRFE_MOUSE	Serotransferrin	Tf	3
NPM_MOUSE	Nucleophosmin	Npm1	2
SPRL1_MOUSE	SPARC-like protein 1	Sparcl1	KA only
HEMO_MOUSE	Hemopexin	Hpx	KA only
NEB2_MOUSE	Neurabin-2	Ppp1r9b	0.33
AGAP2_MOUSE	Arf-GAP with GTPase, ANK repeat and PH domain-containing protein 2	Agap2	0.4
FAK2_MOUSE	Protein-tyrosine kinase 2-beta	Ptk2b	0.4
MTAP2_MOUSE	Microtubule-associated protein 2	Map2	0.53
SRC8_MOUSE	Src substrate cortactin	Cttn	0.53
HOME1_MOUSE	Homer protein homolog 1	Homer1	0.53
NCDN_MOUSE	Neurochondrin	Ncdn	0.66
PROSC_MOUSE	Proline synthase co-transcribed bacterial homolog protein	Prosc	NaCl only
SPB6_MOUSE	Serpin B6	Serpinb6	NaCl only
COR1B_MOUSE	Coronin-1B	Coro1b	NaCl only
EXOC8_MOUSE	Exocyst complex component 8	Exoc8	NaCl only
OAT_MOUSE	Ornithine aminotransferase, mitochondrial	Oat	NaCl only
PSME1_MOUSE	Proteasome activator complex subunit 1	Psme1	NaCl only
ATX10_MOUSE	Ataxin-10	Atxn10	NaCl only
WDR47_MOUSE	WD repeat-containing protein 47	Wdr47	NaCl only
ELMO2_MOUSE	Engulfment and cell motility protein 2	Elmo2	NaCl only
EPN2_MOUSE	Epsin-2	Epn2	NaCl only
SHAN3_MOUSE	SH3 and multiple ankyrin repeat domains protein 3	Shank3	NaCl only

Table 2

3dpi: Differentially expressed proteins (selected)

3dpi: Following comparison of KA vs NaCl-injected mice and statistical analysis (Student *t*-test), proteins that were differentially expressed (fold change≥1.5 or fold ≤0.5) and the differential expression was statistically significant (p≤0.05, Student's *t*-test), according to all 3 quantification approaches (SC, top three TIC and top three PI), were shortlisted. Functional annotation of these proteins at 3dpi using Gene Ontology (biological process), revealed a number of proteins which are related to neuron projection, axon and dendrite development, synaptic plasticity as well as microglial and astrocyte activation. Only proteins present in at least 3 out of 5 samples or uniquely expressed in at least 3 out of 5 KA or NaCl treated mice, were included. Average of the fold change (KA/NaCl) of each quantification approach is shown. Detailed information on mean intensities of all proteins and p values for each quantification approach are shown in Supplementary Table 1.

Table 2: 3dpi: Differentially expressed proteins (selected)			
Entry name	**Protein name**	**Gene name**	**Fold change**
neuron projection, axon and dendrite development and synaptic plasticity			
FLNA_MOUSE	Filamin-A	Flna	6.4
NEB2_MOUSE	Neurabin-2	Ppp1r9b	0.3
MTAP2_MOUSE	Microtubule-associated protein 2	Map2	0.53
MAP1A_MOUSE	Microtubule-associated protein 1A	Map1a	0.6
BAIP2_MOUSE	Brain-specific angiogenesis inhibitor 1-associated protein 2	Baiap2	0.36
SRC8_MOUSE	Src substrate cortactin	Cttn	0.47
SC6A1_MOUSE	Sodium- and chloride-dependent GABA transporter 1	Slc6a1	0.53
AKAP5_MOUSE	A-kinase anchor protein 5	Akap5	NaCl only
BRSK1_MOUSE	Brain-specific serine/threonine-protein kinase 1	Brsk1	NaCl only
SHAN3_MOUSE	SH3 and multiple ankyrin repeat domains protein 3	Shank3	NaCl only
gliosis and inflammation			
MOES_MOUSE	Moesin	Msn	8.3

CLUS_MOUSE	Clusterin	Clu	2.7
VIME_MOUSE	Vimentin	Vim	2.1
GFAP_MOUSE	Glial fibrillary acidic protein	Gfap	1.9
FAK2_MOUSE	Protein-tyrosine kinase 2-beta	Ptk2b	0.36

Table 3

30dpi: differentially expressed proteins (selected)

30dpi: Following comparison of KA vs NaCl-injected mice and statistical analysis (Student *t*-test), proteins that were differentially expressed (fold change≥1.5 or fold ≤0.5) and the differential expression was statistically significant (p≤0.05, Student's *t*-test), according to all 3 quantification approaches (SC, top three TIC and top three PI), were shortlisted. Functional annotation of these proteins at 30dpi using Gene Ontology (biological process), revealed a number of proteins which are related to neuron projection, axon and dendrite development, synaptic plasticity as well as microglial/astrocyte activation and inflammation. Only proteins present in at least 3 out of 5 samples or uniquely expressed in at least 3 out of 5 KA or NaCl treated mice, were included. Average of the fold change (KA/NaCl) of each quantification approach is shown. Detailed information on mean intensities of all proteins and p values for each quantification approach are shown in Supplementary Table 1.

Table 3: 30dpi: differentially expressed proteins (selected)			
neuron projection, axon and dendrite development and synaptic plasticity			
Entry name	**Protein name**	**Gene name**	**Fold change**
FLNA_MOUSE	Filamin-A	Flna	KA only
TENA_MOUSE	Tenascin	Tnc	KA only
USP9X_MOUSE	Probable ubiquitin carboxyl-terminal hydrolase FAF-X	Usp9x	KA only
ITM2C_MOUSE	Integral membrane protein 2C	Itm2c	KA only
MYO6_MOUSE	Unconventional myosin-VI	Myo6	KA only
ANM1_MOUSE	Protein arginine N-methyltransferase 1	Prmt1	KA only
SRC8_MOUSE	Src substrate cortactin	Cttn	0.13
BAIP2_MOUSE	Brain-specific angiogenesis inhibitor 1-associated protein 2	Baiap2	0.16

DBNL_MOUSE	Drebrin-like protein	Dbnl	0.2
PALM_MOUSE	Paralemmin-1	Palm	0.2
DLG2_MOUSE	Disks large homolog 2	Dlg2	0.23
E41L3_MOUSE	Band 4.1-like protein 3	Epb41l3	0.26
DLG4_MOUSE	Disks large homolog 4	Dlg4	0.3
MAP6_MOUSE	Microtubule-associated protein 6	Map6	0.3
PCP4_MOUSE	Purkinje cell protein 4	Pcp4	0.33
SYGP1_MOUSE	Ras/Rap GTPase-activating protein SynGAP	Syngap1	0.33
TAU_MOUSE	Microtubule-associated protein tau	Mapt	0.37
SC6A1_MOUSE	Sodium- and chloride-dependent GABA transporter 1	Slc6a1	0.37
NEB2_MOUSE	Neurabin-2	Ppp1r9b	0.4
AP180_MOUSE	Clathrin coat assembly protein AP180	Snap91	0.4
MAP1B_MOUSE	Microtubule-associated protein 1B	Map1b	0.43
MAP1A_MOUSE	Microtubule-associated protein 1A	Map1a	0.43
MTAP2_MOUSE	Microtubule-associated protein 2	Map2	0.43
PP2BA_MOUSE	Serine/threonine-protein phosphatase 2B catalytic subunit alpha isoform	Ppp3ca	0.5
SYN1_MOUSE	Synapsin-1	Syn1	0.5
SYN2_MOUSE	Synapsin-2	Syn2	0.5
DPYL3_MOUSE	Dihydropyrimidinase-related protein 3	Dpysl3	0.53
MP2K1_MOUSE	Dual specificity mitogen-activated protein kinase kinase 1	Map2k1	0.56
KPCG_MOUSE	Protein kinase C gamma type	Prkcg	0.59
1433F_MOUSE	14-3-3 protein eta	Ywhah	0.59
1433B_MOUSE	14-3-3 protein beta/alpha	Ywhab	0.59
1433T_MOUSE	14-3-3 protein theta	Ywhaq	0.59
1433G_MOUSE	14-3-3 protein gamma	Ywhag	0.63
1433E_MOUSE	14-3-3 protein epsilon	Ywhae	0.66
GRIN1_MOUSE	G protein-regulated inducer of neurite outgrowth 1	Gprin1	NaCl only
LPPR4_MOUSE	Lipid phosphate phosphatase-related protein type 4	Lppr4	NaCl only
NCS1_MOUSE	Neuronal calcium sensor 1	Ncs1	NaCl only
NPTX1_MOUSE	Neuronal pentraxin-1	Nptx1	NaCl only
RPGF2_MOUSE	Rap guanine nucleotide exchange factor 2	Rapgef2	NaCl only
AKAP5_MOUSE	A-kinase anchor protein 5	Akap5	NaCl only
CPLX1_MOUSE	Complexin-1	Cplx1	NaCl only
gliosis and inflammation			
CLUS_MOUSE	Clusterin	Clu	37.5
GFAP_MOUSE	Glial fibrillary acidic protein	Gfap	12.5
VIME_MOUSE	Vimentin	Vim	8
GELS_MOUSE	Gelsolin	Gsn	6.4
APOE_MOUSE	Apolipoprotein E	ApoE	5.2
AL1L1_MOUSE	Aldehyde dehydrogenase 1 family,	Aldh1l1	4.1

	member L1		
CYTC_MOUSE	Cystatin-C	Cst3	4.1
A2MP_MOUSE	Alpha-2-macroglobulin-P	A2m	KA only
AIF1_MOUSE	Allograft inflammatory factor 1	Aif1, Iba1	KA only
C1QT4_MOUSE	Complement C1q tumor necrosis factor-related protein 4	C1qtnf4	KA only
CO4B_MOUSE	Complement C4-B	C4b	KA only
CD44_MOUSE	CD44 antigen	Cd44	KA only
CD9_MOUSE	CD9 antigen	CD9	KA only
HA17_MOUSE	H-2 class I histocompatibility antigen, Q7 alpha chain	H2-Q7	KA only
ITAV_MOUSE	Integrin alpha-V	Itgav	KA only
ITB2_MOUSE	Integrin beta-2	Itgb2	KA only
PLSL_MOUSE	Plastin-2	Lcp1	KA only
PAFA_MOUSE	Platelet-activating factor acetylhydrolase	Pla2g7	KA only
S10A1_MOUSE	Protein S100-A1	S100a1	KA only
S10A6_MOUSE	Protein S100-A6	S100a6	KA only
LEG1_MOUSE	Galectin-1	Lgals1	KA only
NEB2_MOUSE	Neurabin-2	Ppp1r9b	0.4
PP2BB_MOUSE	Serine/threonine-protein phosphatase 2B catalytic subunit beta isoform	Ppp3cb	0.47

Table 4

Consistently differentially expressed proteins (in more than one time-point). Proteins that are consistently differentially expressed in more than one timepoint are presented in this table. Average of the ratio (KA/NaCl) of the three quantification approaches is shown. Detailed information on mean intensities of all proteins and p values (p values≤0.05) for each quantification approach are shown in Supplementary Table 1.

Table 4: Consistently differentially expressed proteins (in more than one timepoint)

Gene	Protein	1dpi	3dpi	30dpi
Trf	Serotransferrin	3	2.9	3.7
Map2	Microtubule-associated protein 2	0.53	0.53	0.43
Cttn	Src substrate cortactin	0.47	0.47	0.13
Ptk2b	Protein-tyrosine kinase 2-beta	0.4	0.37	Detected-no difference
Ppp1r9b	Neurabin-2	0.33	0.3	0.4

Prosc	Proline synthase co-transcribed bacterial homolog protein	NaCl only	Detected-no difference	KA only
Psme1	Proteasome activator complex subunit 1	NaCl only	-	KA only
Shank3	SH3 and multiple ankyrin repeat domains protein 3	NaCl only	NaCl only	-
Gfap	Glial fibrillary acidic protein	Detected-no difference	1.9	12.5
Vim	Vimentin	Detected-no difference	2	8
Clu	Clusterin	Detected-no difference	2.7	37.5
Dhrs1	Dehydrogenase/reductase SDR family member 1	-	2.6	16.2
Flna	Filamin-A	-	6.4	KA only
Hexb	Beta-hexosaminidase subunit beta	-	2.2	KA only
Map1a	Microtubule-associated protein 1A	Detected-no difference	0.6	0.43
Aak1	AP2-associated protein kinase 1	Detected-no difference	0.43	0.3
Baiap2	Brain-specific angiogenesis inhibitor 1-associated protein 2	Detected-no difference	0.36	0.16
Rph3a	Rabphilin-3A	Detected-no difference	0.53	0.3
Slc6a1	Sodium- and chloride-dependent GABA transporter 1	Detected-no difference	0.53	0.37
G3bp2	Ras GTPase-activating protein-binding protein 2	-	0.43	NaCl only
Apod	Apolipoprotein D	-	KA only	KA only
Tgm1	Protein-glutamine gamma-glutamyltransferase K	-	KA only	KA only
Capg	Macrophage-capping protein	-	KA only	KA only
Ctsz	Cathepsin Z	-	KA only	KA only
Akap5	A-kinase anchor protein 5	-	NaCl only	NaCl only

Table 5

Validation of selected findings by MRM LC-MS/MS

Validation of selected findings by MRM LC-MS/MS approach. Upregulation of selected differentially expressed proteins at 30dpi from the LC-MS/MS analysis was

verified by targeted MRM approach (n=5/group). The ratio of the intensities (sum of transitions) of each peptide and the corresponding p values (Student *t*-test) are shown, in parallel to the respective ratios and p values of the LC-MS/MS analysis. Detailed information on the mean intensities of the peptides of each sample are shown in Supplementary Table 3.

Table 5: Validation of selected findings by MRM LC-MS/MS

	LC-MS/MS data		MRM data		
Protein	**KA/NaCl**	***t*-test**	**Peptides**	**KA/NaCl**	***t*-test**
GFAP	**12.5**	**0.01**	AAELNQLR	**6.1**	**0.01**
			DNFAQDLGTLR	**2.3**	**0.03**
			LEAENNLAAYR	**9.9**	**0.01**
Apolipo-protein E	**5.2**	**0.01**	MEEQTQQIR	**4.6**	**0.01**
			TANLGAGAAQPLR	**2.1**	**0.12**
Clusterin	**37.5**	**0.01**	LFDSDPITVVLPEEVSK	**2.6**	**0.02**
Vimentin	**7.9**	**0.01**	EEAESTLQSFR	**6.4**	**0.01**
Cystatin-C	**4.1**	**0.03**	GSNDAYHSR	**3.5**	**0.10**
Galectin-1	**KA only**		FNAHGDANTIVCNTK	**11.3**	**0.01**
Gelsolin	**6.4**	**0.01**	SEDCFILDHGR	**5.5**	**0.01**
Homer-1 (control)	**0.8**	**0.15**	TQALSHASSAISK	**0.8**	**0.19**

Table 6

Validation of proteomic findings in other studies of human/mouse MTLE samples. In order to correlate our mouse model to the human MTLE syndrome, we crosschecked our proteomic findings in existing studies of human MTLE samples. Several of our proteomic findings have been confirmed by microarray or proteomics 2 dimensional electrophoresis (2DE) studies using human samples. In addition, proteomic changes reported in our study were also observed in other studies using the KA mouse model of MTLE, mainly by immunohistochemistry.

Table 6: Validation of proteomic findings in other studies of human/mouse MTLE samples

	Proteomic findings			Other studies
Protein name	**1dpi**	**3dpi**	**30dpi**	
				Lee et al 2007 [51] (human TLE hippocampi - microarrays)
GFAP	detected/ no diff	up (1.9)	up (12.5)	up
GMP reductase 1	-	-	KA only	up
Moesin	-	8.3	-	up
DLG4	-	-	down (0.3)	down
CD44	-	-	KA only	up
Homer 1	down (0.53)	-	-	down
Synapsin-1	detected/ no diff	detected/ no diff	0.5	down
MAP2K4	-	NaCl only	-	down
PTK2B (FAK2)	down (0.4)	down (0.36)	detected/ no diff	down
				Arion et al 2006 [93] (human temporal cortical samples - microarrays)
Serotransferrin	up (3)	up (2.9)	up (3.7)	up (1.9)
				Jamali et al 2006 [92] (human MTLE entorhinal cortex - microarrays)
Tenascin	-	-	KA only	up
				Venugopal et al 2012 [12] (human TLE samples-microarrays)
Amphiphysin	-	-	down (0.43)	down
				Yang et al 2006 [94] (human MTLE hippocampus-proteomics 2DE gels)
Ezrin	-	-	up (5.3)	up (3)
Map2k1	-	-	down (0.55)	down (0.33)
				Jessberger et al 2003 [50] (mouse KA MTLE model – IHC)
Homer 1	down (0.53)	-	-	up
				Heinrich et al 2006 [15] (mouse KA MTLE model – IHC)
GFAP	detected/ no diff	up (1.9)	up (12.5)	7dpi up, 14dpi up, 21dpi up, 6wpi up
Vimentin	-	up (2.1)	up (8.0)	21dpi up
Iba-1	-	-	KA only	7dpi up
				Pernot et al 2011[25] (mouse KA MTLE model – IHC)
GFAP	detected/	up (1.9)	up (12.5)	3dpi up, 7dpi up, 21dpi up

	no diff			
				Zattoni et al 2011 [9595] (mouse KA MTLE model – IHC)
Iba-1	-	-	KA only	14dpi up

Supporting Information: Sample variance (Supplementary Figure 1), Reproducibility of protein identifications in KA and NaCl-injected animals at 1, 3 and 30dpi (Supplementary figure 2); Overlap of differentially expressed proteins among the three quantification approaches (Supplementary figure 3); All proteins and differentially expressed proteins quantified per time-point (Supplementary table 1); MRM method development (Supplementary table 2); MRM quantification data (Supplementary table 3)

ACKNOWLEDGEMENTS

VB, VD, JSA, CR, MM, GM, PS, AD and AV received funding from the European Community's Framework program Neurinox (Health-F2-2011-278611). WM received institutional funds. We would like to thank Claire Beaup (Inserm, Grenoble, France) for technical assistance.

REFERENCES

1. Mathern, G. W.; Pretorius, J. K.; Babb, T. L. Influence of the type of initial precipitating injury and at what age it occurs on course and outcome in patients with temporal lobe seizures. *J Neurosurg* **1995,** 82 (2), 220-7.
2. Mathern, G. W.; Babb, T. L.; Leite, J. P.; Pretorius, K.; Yeoman, K. M.; Kuhlman, P. A. The pathogenic and progressive features of chronic human hippocampal epilepsy. *Epilepsy Res* **1996,** 26 (1), 151-61.
3. Engel, J., Jr. Mesial temporal lobe epilepsy: what have we learned? *Neuroscientist* **2001,** 7 (4), 340-52.
4. Cendes, F.; Andermann, F.; Dubeau, F.; Gloor, P.; Evans, A.; Jones-Gotman, M.; Olivier, A.; Andermann, E.; Robitaille, Y.; Lopes-Cendes, I.; et al. Early childhood prolonged febrile convulsions, atrophy and sclerosis of mesial structures, and temporal lobe epilepsy: an MRI volumetric study. *Neurology* **1993,** 43 (6), 1083-7.
5. Pitkanen, A.; Lukasiuk, K. Mechanisms of epileptogenesis and potential treatment targets. *Lancet Neurol* **2011,** 10 (2), 173-86.

6. Hunsberger, J. G.; Bennett, A. H.; Selvanayagam, E.; Duman, R. S.; Newton, S. S. Gene profiling the response to kainic acid induced seizures. *Brain Res Mol Brain Res* **2005,** 141 (1), 95-112.
7. Sharma, A. K.; Searfoss, G. H.; Reams, R. Y.; Jordan, W. H.; Snyder, P. W.; Chiang, A. Y.; Jolly, R. A.; Ryan, T. P. Kainic acid-induced F-344 rat model of mesial temporal lobe epilepsy: gene expression and canonical pathways. *Toxicol Pathol* **2009,** 37 (6), 776-89.
8. Lauren, H. B.; Lopez-Picon, F. R.; Brandt, A. M.; Rios-Rojas, C. J.; Holopainen, I. E. Transcriptome analysis of the hippocampal CA1 pyramidal cell region after kainic acid-induced status epilepticus in juvenile rats. *PLoS One* **2010,** 5 (5), e10733.
9. Okamoto, O. K.; Janjoppi, L.; Bonone, F. M.; Pansani, A. P.; da Silva, A. V.; Scorza, F. A.; Cavalheiro, E. A. Whole transcriptome analysis of the hippocampus: toward a molecular portrait of epileptogenesis. *BMC Genomics* **2010,** 11, 230.
10. Gorter, J. A.; van Vliet, E. A.; Aronica, E.; Breit, T.; Rauwerda, H.; Lopes da Silva, F. H.; Wadman, W. J. Potential new antiepileptogenic targets indicated by microarray analysis in a rat model for temporal lobe epilepsy. *J Neurosci* **2006,** 26 (43), 11083-110.
11. Motti, D.; Le Duigou, C.; Eugene, E.; Chemaly, N.; Wittner, L.; Lazarevic, D.; Krmac, H.; Marstrand, T.; Valen, E.; Sanges, R.; et al. Gene expression analysis of the emergence of epileptiform activity after focal injection of kainic acid into mouse hippocampus. *Eur J Neurosci* **2010,** 32 (8), 1364-79.
12. Venugopal, A. K.; Sameer Kumar, G. S.; Mahadevan, A.; Selvan, L. D.; Marimuthu, A.; Dikshit, J. B.; Tata, P.; Ramachandra, Y.; Chaerkady, R.; Sinha, S.; et al. Transcriptomic Profiling of Medial Temporal Lobe Epilepsy. *J Proteomics Bioinform* **2012,** 5 (2).
13. Bouilleret, V.; Ridoux, V.; Depaulis, A.; Marescaux, C.; Nehlig, A.; Le Gal La Salle, G. Recurrent seizures and hippocampal sclerosis following intrahippocampal kainate injection in adult mice: electroencephalography, histopathology and synaptic reorganization similar to mesial temporal lobe epilepsy. *Neuroscience* **1999,** 89 (3), 717-29.
14. Riban, V.; Bouilleret, V.; Pham-Le, B. T.; Fritschy, J. M.; Marescaux, C.; Depaulis, A. Evolution of hippocampal epileptic activity during the development of hippocampal sclerosis in a mouse model of temporal lobe epilepsy. *Neuroscience* **2002,** 112 (1), 101-11.
15. Heinrich, C.; Nitta, N.; Flubacher, A.; Muller, M.; Fahrner, A.; Kirsch, M.; Freiman, T.; Suzuki, F.; Depaulis, A.; Frotscher, M.; et al. Reelin deficiency and displacement of mature neurons, but not neurogenesis, underlie the formation of granule cell dispersion in the epileptic hippocampus. *J Neurosci* **2006,** 26 (17), 4701-13.
16. Heinrich, C.; Lahteinen, S.; Suzuki, F.; Anne-Marie, L.; Huber, S.; Haussler, U.; Haas, C.; Larmet, Y.; Castren, E.; Depaulis, A. Increase in BDNF-mediated TrkB signaling promotes epileptogenesis in a mouse model of mesial temporal lobe epilepsy. *Neurobiol Dis* **2011,** 42 (1), 35-47.
17. Meier, R.; Haussler, U.; Aertsen, A.; Deransart, C.; Depaulis, A.; Egert, U. Short-term changes in bilateral hippocampal coherence precede epileptiform events. *Neuroimage* **2007,** 38 (1), 138-49.
18. Kralic, J. E.; Ledergerber, D. A.; Fritschy, J. M. Disruption of the neurogenic potential of the dentate gyrus in a mouse model of temporal lobe epilepsy with focal seizures. *Eur J Neurosci* **2005,** 22 (8), 1916-27.

19. Wang, W.; Zhou, H.; Lin, H.; Roy, S.; Shaler, T. A.; Hill, L. R.; Norton, S.; Kumar, P.; Anderle, M.; Becker, C. H. Quantification of proteins and metabolites by mass spectrometry without isotopic labeling or spiked standards. *Anal Chem* **2003,** 75 (18), 4818-26.
20. Bantscheff, M.; Schirle, M.; Sweetman, G.; Rick, J.; Kuster, B. Quantitative mass spectrometry in proteomics: a critical review. *Anal Bioanal Chem* **2007,** 389 (4), 1017-31.
21. Freund, D. M.; Prenni, J. E. Improved Detection of Quantitative Differences Using a Combination of Spectral Counting and MS/MS Total Ion Current. *J Proteome Res* **2013,** 12 (4), 1996-2004.
22. Grossmann, J.; Roschitzki, B.; Panse, C.; Fortes, C.; Barkow-Oesterreicher, S.; Rutishauser, D.; Schlapbach, R. Implementation and evaluation of relative and absolute quantification in shotgun proteomics with label-free methods. *J Proteomics* **2010,** 73 (9), 1740-6.
23. Old, W. M.; Meyer-Arendt, K.; Aveline-Wolf, L.; Pierce, K. G.; Mendoza, A.; Sevinsky, J. R.; Resing, K. A.; Ahn, N. G. Comparison of label-free methods for quantifying human proteins by shotgun proteomics. *Mol Cell Proteomics* **2005,** 4 (10), 1487-502.
24. Ahrne, E.; Molzahn, L.; Glatter, T.; Schmidt, A. Critical assessment of proteome-wide label-free absolute abundance estimation strategies. *Proteomics* **2013,** 13 (17), 2567-78.
25. Pernot, F.; Heinrich, C.; Barbier, L.; Peinnequin, A.; Carpentier, P.; Dhote, F.; Baille, V.; Beaup, C.; Depaulis, A.; Dorandeu, F. Inflammatory changes during epileptogenesis and spontaneous seizures in a mouse model of mesiotemporal lobe epilepsy. *Epilepsia* **2011,** 52 (12), 2315-25.
26. Nitta, N.; Heinrich, C.; Hirai, H.; Suzuki, F. Granule cell dispersion develops without neurogenesis and does not fully depend on astroglial cell generation in a mouse model of temporal lobe epilepsy. *Epilepsia* **2008,** 49 (10), 1711-22.
27. Wisniewski, J. R.; Zougman, A.; Nagaraj, N.; Mann, M. Universal sample preparation method for proteome analysis. *Nat Methods* **2009,** 6 (5), 359-62.
28. Keller, A.; Nesvizhskii, A. I.; Kolker, E.; Aebersold, R. Empirical statistical model to estimate the accuracy of peptide identifications made by MS/MS and database search. *Anal Chem* **2002,** 74 (20), 5383-92.
29. Nesvizhskii, A. I.; Keller, A.; Kolker, E.; Aebersold, R. A statistical model for identifying proteins by tandem mass spectrometry. *Anal Chem* **2003,** 75 (17), 4646-58.
30. MacLean, B.; Tomazela, D. M.; Shulman, N.; Chambers, M.; Finney, G. L.; Frewen, B.; Kern, R.; Tabb, D. L.; Liebler, D. C.; MacCoss, M. J. Skyline: an open source document editor for creating and analyzing targeted proteomics experiments. *Bioinformatics* **2010,** 26 (7), 966-8.
31. Desiere, F.; Deutsch, E. W.; King, N. L.; Nesvizhskii, A. I.; Mallick, P.; Eng, J.; Chen, S.; Eddes, J.; Loevenich, S. N.; Aebersold, R. The PeptideAtlas project. *Nucleic Acids Res* **2006,** 34 (Database issue), D655-8.
32. Sofroniew, M. V. Molecular dissection of reactive astrogliosis and glial scar formation. *Trends Neurosci* **2009,** 32 (12), 638-47.
33. Robel, S.; Berninger, B.; Gotz, M. The stem cell potential of glia: lessons from reactive gliosis. *Nat Rev Neurosci* **2011,** 12 (2), 88-104.
34. Seifert, G.; Schilling, K.; Steinhauser, C. Astrocyte dysfunction in neurological disorders: a molecular perspective. *Nat Rev Neurosci* **2006,** 7 (3), 194-206.

35. Bramanti, V.; Tomassoni, D.; Avitabile, M.; Amenta, F.; Avola, R. Biomarkers of glial cell proliferation and differentiation in culture. *Front Biosci (Schol Ed)* **2010,** 2, 558-70.
36. Wang, H.; Nong, Y.; Bazan, F.; Greengard, P.; Flajolet, M. Norbin: A promising central nervous system regulator. *Commun Integr Biol* **2010,** 3 (6), 487-90.
37. Bloom, O.; Unternaehrer, J. J.; Jiang, A.; Shin, J. S.; Delamarre, L.; Allen, P.; Mellman, I. Spinophilin participates in information transfer at immunological synapses. *J Cell Biol* **2008,** 181 (2), 203-11.
38. Cavarsan, C. F.; Tescarollo, F.; Tesone-Coelho, C.; Morais, R. L.; Motta, F. L.; Blanco, M. M.; Mello, L. E. Pilocarpine-induced status epilepticus increases Homer1a and changes mGluR5 expression. *Epilepsy Res* **2012,** 101 (3), 253-60.
39. Waragai, M.; Nagamitsu, S.; Xu, W.; Li, Y. J.; Lin, X.; Ashizawa, T. Ataxin 10 induces neuritogenesis via interaction with G-protein beta2 subunit. *J Neurosci Res* **2006,** 83 (7), 1170-8.
40. Bertaso, F.; Roussignol, G.; Worley, P.; Bockaert, J.; Fagni, L.; Ango, F. Homer1a-dependent crosstalk between NMDA and metabotropic glutamate receptors in mouse neurons. *PLoS One* **2010,** 5 (3), e9755.
41. Wang, W.; Lundin, V. F.; Millan, I.; Zeng, A.; Chen, X.; Yang, J.; Allen, E.; Chen, N.; Bach, G.; Hsu, A.; et al. Nemitin, a novel Map8/Map1s interacting protein with Wd40 repeats. *PLoS One* **2012,** 7 (4), e33094.
42. Pfister, J. A.; D'Mello, S. R. Insights into the regulation of neuronal viability by nucleophosmin/B23. *Exp Biol Med (Maywood)* **2015,** 240 (6), 774-86.
43. Gongidi, V.; Ring, C.; Moody, M.; Brekken, R.; Sage, E. H.; Rakic, P.; Anton, E. S. SPARC-like 1 regulates the terminal phase of radial glia-guided migration in the cerebral cortex. *Neuron* **2004,** 41 (1), 57-69.
44. Li, R. C.; Saleem, S.; Zhen, G.; Cao, W.; Zhuang, H.; Lee, J.; Smith, A.; Altruda, F.; Tolosano, E.; Dore, S. Heme-hemopexin complex attenuates neuronal cell death and stroke damage. *J Cereb Blood Flow Metab* **2009,** 29 (5), 953-64.
45. Mi, H.; Poudel, S.; Muruganujan, A.; Casagrande, J. T.; Thomas, P. D. PANTHER version 10: expanded protein families and functions, and analysis tools. *Nucleic Acids Res* **2016,** 44 (D1), D336-42.
46. Bindea, G.; Mlecnik, B.; Hackl, H.; Charoentong, P.; Tosolini, M.; Kirilovsky, A.; Fridman, W. H.; Pages, F.; Trajanoski, Z.; Galon, J. ClueGO: a Cytoscape plug-in to decipher functionally grouped gene ontology and pathway annotation networks. *Bioinformatics* **2009,** 25 (8), 1091-3.
47. Duveau, V.; Pouyatos, B.; Bressand, K.; Bouyssieres, C.; Chabrol, T.; Roche, Y.; Depaulis, A.; Roucard, C. Differential Effects of Antiepileptic Drugs on Focal Seizures in the Intrahippocampal Kainate Mouse Model of Mesial Temporal Lobe Epilepsy. *CNS Neurosci Ther* **2016**.
48. Tu, C.; Li, J.; Sheng, Q.; Zhang, M.; Qu, J. Systematic assessment of survey scan and MS2-based abundance strategies for label-free quantitative proteomics using high-resolution MS data. *J Proteome Res* **2014,** 13 (4), 2069-79.
49. Ning, K.; Fermin, D.; Nesvizhskii, A. I. Comparative analysis of different label-free mass spectrometry based protein abundance estimates and their correlation with RNA-Seq gene expression data. *J Proteome Res* **2012,** 11 (4), 2261-71.
50. Jessberger, S.; Kempermann, G. Adult-born hippocampal neurons mature into activity-dependent responsiveness. *Eur J Neurosci* **2003,** 18 (10), 2707-12.
51. Lee, T. S.; Mane, S.; Eid, T.; Zhao, H.; Lin, A.; Guan, Z.; Kim, J. H.; Schweitzer, J.; King-Stevens, D.; Weber, P.; et al. Gene expression in temporal lobe

epilepsy is consistent with increased release of glutamate by astrocytes. *Mol Med* **2007,** 13 (1-2), 1-13.
52. Qing, Y.; Yingmao, G.; Lujun, B.; Shaoling, L. Role of Npm1 in proliferation, apoptosis and differentiation of neural stem cells. *J Neurol Sci* **2008,** 266 (1-2), 131-7.
53. Zhang, X.; Cui, S. S.; Wallace, A. E.; Hannesson, D. K.; Schmued, L. C.; Saucier, D. M.; Honer, W. G.; Corcoran, M. E. Relations between brain pathology and temporal lobe epilepsy. *J Neurosci* **2002,** 22 (14), 6052-61.
54. Sawallisch, C.; Berhorster, K.; Disanza, A.; Mantoani, S.; Kintscher, M.; Stoenica, L.; Dityatev, A.; Sieber, S.; Kindler, S.; Morellini, F.; et al. The insulin receptor substrate of 53 kDa (IRSp53) limits hippocampal synaptic plasticity. *J Biol Chem* **2009,** 284 (14), 9225-36.
55. Bockmann, J.; Kreutz, M. R.; Gundelfinger, E. D.; Bockers, T. M. ProSAP/Shank postsynaptic density proteins interact with insulin receptor tyrosine kinase substrate IRSp53. *J Neurochem* **2002,** 83 (4), 1013-7.
56. Inoue, E.; Mochida, S.; Takagi, H.; Higa, S.; Deguchi-Tawarada, M.; Takao-Rikitsu, E.; Inoue, M.; Yao, I.; Takeuchi, K.; Kitajima, I.; et al. SAD: a presynaptic kinase associated with synaptic vesicles and the active zone cytomatrix that regulates neurotransmitter release. *Neuron* **2006,** 50 (2), 261-75.
57. Zhang, M.; Patriarchi, T.; Stein, I. S.; Qian, H.; Matt, L.; Nguyen, M.; Xiang, Y. K.; Hell, J. W. Adenylyl cyclase anchoring by a kinase anchor protein AKAP5 (AKAP79/150) is important for postsynaptic beta-adrenergic signaling. *J Biol Chem* **2013,** 288 (24), 17918-31.
58. Chen, Y. K.; Hsueh, Y. P. Cortactin-binding protein 2 modulates the mobility of cortactin and regulates dendritic spine formation and maintenance. *J Neurosci* **2012,** 32 (3), 1043-55.
59. Cassimeris, L.; Spittle, C. Regulation of microtubule-associated proteins. *Int Rev Cytol* **2001,** 210, 163-226.
60. Schwartz, M.; Baruch, K. The resolution of neuroinflammation in neurodegeneration: leukocyte recruitment via the choroid plexus. *EMBO J* **2014,** 33 (1), 7-22.
61. Vezzani, A.; French, J.; Bartfai, T.; Baram, T. Z. The role of inflammation in epilepsy. *Nat Rev Neurol* **2011,** 7 (1), 31-40.
62. Gonzalez-Billault, C.; Engelke, M.; Jimenez-Mateos, E. M.; Wandosell, F.; Caceres, A.; Avila, J. Participation of structural microtubule-associated proteins (MAPs) in the development of neuronal polarity. *J Neurosci Res* **2002,** 67 (6), 713-9.
63. Tortosa, E.; Montenegro-Venegas, C.; Benoist, M.; Hartel, S.; Gonzalez-Billault, C.; Esteban, J. A.; Avila, J. Microtubule-associated protein 1B (MAP1B) is required for dendritic spine development and synaptic maturation. *J Biol Chem* **2011,** 286 (47), 40638-48.
64. Denarier, E.; Fourest-Lieuvin, A.; Bosc, C.; Pirollet, F.; Chapel, A.; Margolis, R. L.; Job, D. Nonneuronal isoforms of STOP protein are responsible for microtubule cold stability in mammalian fibroblasts. *Proc Natl Acad Sci U S A* **1998,** 95 (11), 6055-60.
65. Haeckel, A.; Ahuja, R.; Gundelfinger, E. D.; Qualmann, B.; Kessels, M. M. The actin-binding protein Abp1 controls dendritic spine morphology and is important for spine head and synapse formation. *J Neurosci* **2008,** 28 (40), 10031-44.
66. Arstikaitis, P.; Gauthier-Campbell, C.; Carolina Gutierrez Herrera, R.; Huang, K.; Levinson, J. N.; Murphy, T. H.; Kilimann, M. W.; Sala, C.; Colicos, M. A.; El-Husseini, A. Paralemmin-1, a modulator of filopodia induction is required for spine maturation. *Mol Biol Cell* **2008,** 19 (5), 2026-38.

67. Suzuki, F.; Heinrich, C.; Boehrer, A.; Mitsuya, K.; Kurokawa, K.; Matsuda, M.; Depaulis, A. Glutamate receptor antagonists and benzodiazepine inhibit the progression of granule cell dispersion in a mouse model of mesial temporal lobe epilepsy. *Epilepsia* **2005,** 46 (2), 193-202.
68. Barnett, M. E.; Madgwick, D. K.; Takemoto, D. J. Protein kinase C as a stress sensor. *Cell Signal* **2007,** 19 (9), 1820-9.
69. Li, L.; You, L.; Sunyer, B.; Patil, S.; Hoger, H.; Pollak, A.; Stork, O.; Lubec, G. Hippocampal protein kinase C family members in spatial memory retrieval in the mouse. *Behav Brain Res* **2014,** 258, 202-7.
70. Aronica, E.; Ravizza, T.; Zurolo, E.; Vezzani, A. Astrocyte immune responses in epilepsy. *Glia* **2012,** 60 (8), 1258-68.
71. Steinhauser, C.; Seifert, G.; Bedner, P. Astrocyte dysfunction in temporal lobe epilepsy: K+ channels and gap junction coupling. *Glia* **2012,** 60 (8), 1192-202.
72. Eng, L. F.; Vanderhaeghen, J. J.; Bignami, A.; Gerstl, B. An acidic protein isolated from fibrous astrocytes. *Brain Res* **1971,** 28 (2), 351-4.
73. Weiss, K. H.; Johanssen, C.; Tielsch, A.; Herz, J.; Deller, T.; Frotscher, M.; Forster, E. Malformation of the radial glial scaffold in the dentate gyrus of reeler mice, scrambler mice, and ApoER2/VLDLR-deficient mice. *J Comp Neurol* **2003,** 460 (1), 56-65.
74. Campbell, K.; Gotz, M. Radial glia: multi-purpose cells for vertebrate brain development. *Trends Neurosci* **2002,** 25 (5), 235-8.
75. Charnay, Y.; Imhof, A.; Vallet, P. G.; Kovari, E.; Bouras, C.; Giannakopoulos, P. Clusterin in neurological disorders: molecular perspectives and clinical relevance. *Brain Res Bull* **2012,** 88 (5), 434-43.
76. LaDu, M. J.; Shah, J. A.; Reardon, C. A.; Getz, G. S.; Bu, G.; Hu, J.; Guo, L.; Van Eldik, L. J. Apolipoprotein E and apolipoprotein E receptors modulate A beta-induced glial neuroinflammatory responses. *Neurochem Int* **2001,** 39 (5-6), 427-34.
77. Guo, L.; LaDu, M. J.; Van Eldik, L. J. A dual role for apolipoprotein e in neuroinflammation: anti- and pro-inflammatory activity. *J Mol Neurosci* **2004,** 23 (3), 205-12.
78. Dong, J. H.; Ying, G. X.; Liu, X.; Wang, W. Y.; Wang, Y.; Ni, Z. M.; Zhou, C. F. Lesion-induced gelsolin upregulation in the hippocampus following entorhinal deafferentation. *Hippocampus* **2006,** 16 (1), 91-100.
79. Zhang, Q. H.; Chen, Q.; Kang, J. R.; Liu, C.; Dong, N.; Zhu, X. M.; Sheng, Z. Y.; Yao, Y. M. Treatment with gelsolin reduces brain inflammation and apoptotic signaling in mice following thermal injury. *J Neuroinflammation* **2011,** 8, 118.
80. Yang, Y.; Vidensky, S.; Jin, L.; Jie, C.; Lorenzini, I.; Frankl, M.; Rothstein, J. D. Molecular comparison of GLT1+ and ALDH1L1+ astrocytes in vivo in astroglial reporter mice. *Glia* **2011,** 59 (2), 200-7.
81. Ohsawa, K.; Imai, Y.; Sasaki, Y.; Kohsaka, S. Microglia/macrophage-specific protein Iba1 binds to fimbrin and enhances its actin-bundling activity. *J Neurochem* **2004,** 88 (4), 844-56.
82. Mika, J. Modulation of microglia can attenuate neuropathic pain symptoms and enhance morphine effectiveness. *Pharmacol Rep* **2008,** 60 (3), 297-307.
83. Hattori, M.; Kusakabe, S.; Ohgusu, H.; Tsuchiya, Y.; Ito, T.; Sakaki, Y. Structure of the rat alpha 2-macroglobulin-coding gene. *Gene* **1989,** 77 (2), 333-40.
84. Plachta, N.; Annaheim, C.; Bissiere, S.; Lin, S.; Ruegg, M.; Hoving, S.; Muller, D.; Poirier, F.; Bibel, M.; Barde, Y. A. Identification of a lectin causing the degeneration of neuronal processes using engineered embryonic stem cells. *Nat Neurosci* **2007,** 10 (6), 712-9.

85. Kurihara, D.; Ueno, M.; Tanaka, T.; Yamashita, T. Expression of galectin-1 in immune cells and glial cells after spinal cord injury. *Neurosci Res* **2010,** 66 (3), 265-70.
86. Pirttila, T. J.; Lukasiuk, K.; Hakansson, K.; Grubb, A.; Abrahamson, M.; Pitkanen, A. Cystatin C modulates neurodegeneration and neurogenesis following status epilepticus in mouse. *Neurobiol Dis* **2005,** 20 (2), 241-53.
87. Gore, Y.; Starlets, D.; Maharshak, N.; Becker-Herman, S.; Kaneyuki, U.; Leng, L.; Bucala, R.; Shachar, I. Macrophage migration inhibitory factor induces B cell survival by activation of a CD74-CD44 receptor complex. *J Biol Chem* **2008,** 283 (5), 2784-92.
88. Pavlick, K. P.; Ostanin, D. V.; Furr, K. L.; Laroux, F. S.; Brown, C. M.; Gray, L.; Kevil, C. G.; Grisham, M. B. Role of T-cell-associated lymphocyte function-associated antigen-1 in the pathogenesis of experimental colitis. *Int Immunol* **2006,** 18 (2), 389-98.
89. Tjoelker, L. W.; Eberhardt, C.; Unger, J.; Trong, H. L.; Zimmerman, G. A.; McIntyre, T. M.; Stafforini, D. M.; Prescott, S. M.; Gray, P. W. Plasma platelet-activating factor acetylhydrolase is a secreted phospholipase A2 with a catalytic triad. *J Biol Chem* **1995,** 270 (43), 25481-7.
90. Guillemain, I.; Kahane, P.; Depaulis, A. Animal models to study aetiopathology of epilepsy: what are the features to model? *Epileptic Disord* **2012,** 14 (3), 217-25.
91. Depaulis, A.; Hamelin, S. Animal models for mesiotemporal lobe epilepsy: The end of a misunderstanding? *Rev Neurol (Paris)* **2015,** 171 (3), 217-26.
92. Jamali, S.; Bartolomei, F.; Robaglia-Schlupp, A.; Massacrier, A.; Peragut, J. C.; Regis, J.; Dufour, H.; Ravid, R.; Roll, P.; Pereira, S.; et al. Large-scale expression study of human mesial temporal lobe epilepsy: evidence for dysregulation of the neurotransmission and complement systems in the entorhinal cortex. *Brain* **2006,** 129 (Pt 3), 625-41.
93. Arion, D.; Sabatini, M.; Unger, T.; Pastor, J.; Alonso-Nanclares, L.; Ballesteros-Yanez, I.; Garcia Sola, R.; Munoz, A.; Mirnics, K.; DeFelipe, J. Correlation of transcriptome profile with electrical activity in temporal lobe epilepsy. *Neurobiol Dis* **2006,** 22 (2), 374-87.
94. Yang, J. W.; Czech, T.; Felizardo, M.; Baumgartner, C.; Lubec, G. Aberrant expression of cytoskeleton proteins in hippocampus from patients with mesial temporal lobe epilepsy. *Amino Acids* **2006,** 30 (4), 477-93.
95. Zattoni, M.; Mura, M. L.; Deprez, F.; Schwendener, R. A.; Engelhardt, B.; Frei, K.; Fritschy, J. M. Brain infiltration of leukocytes contributes to the pathophysiology of temporal lobe epilepsy. *J Neurosci* **2011,** 31 (11), 4037-50.

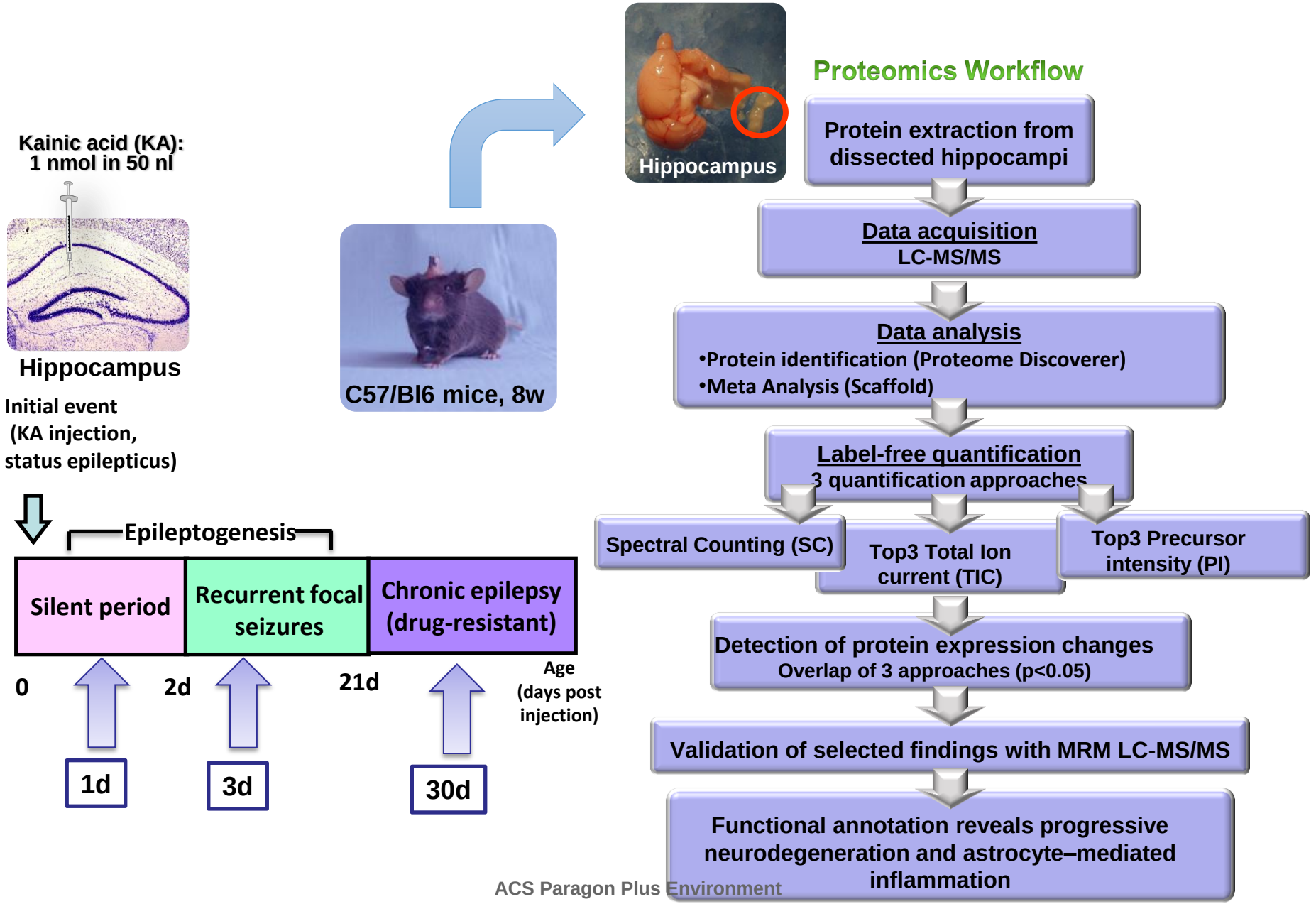

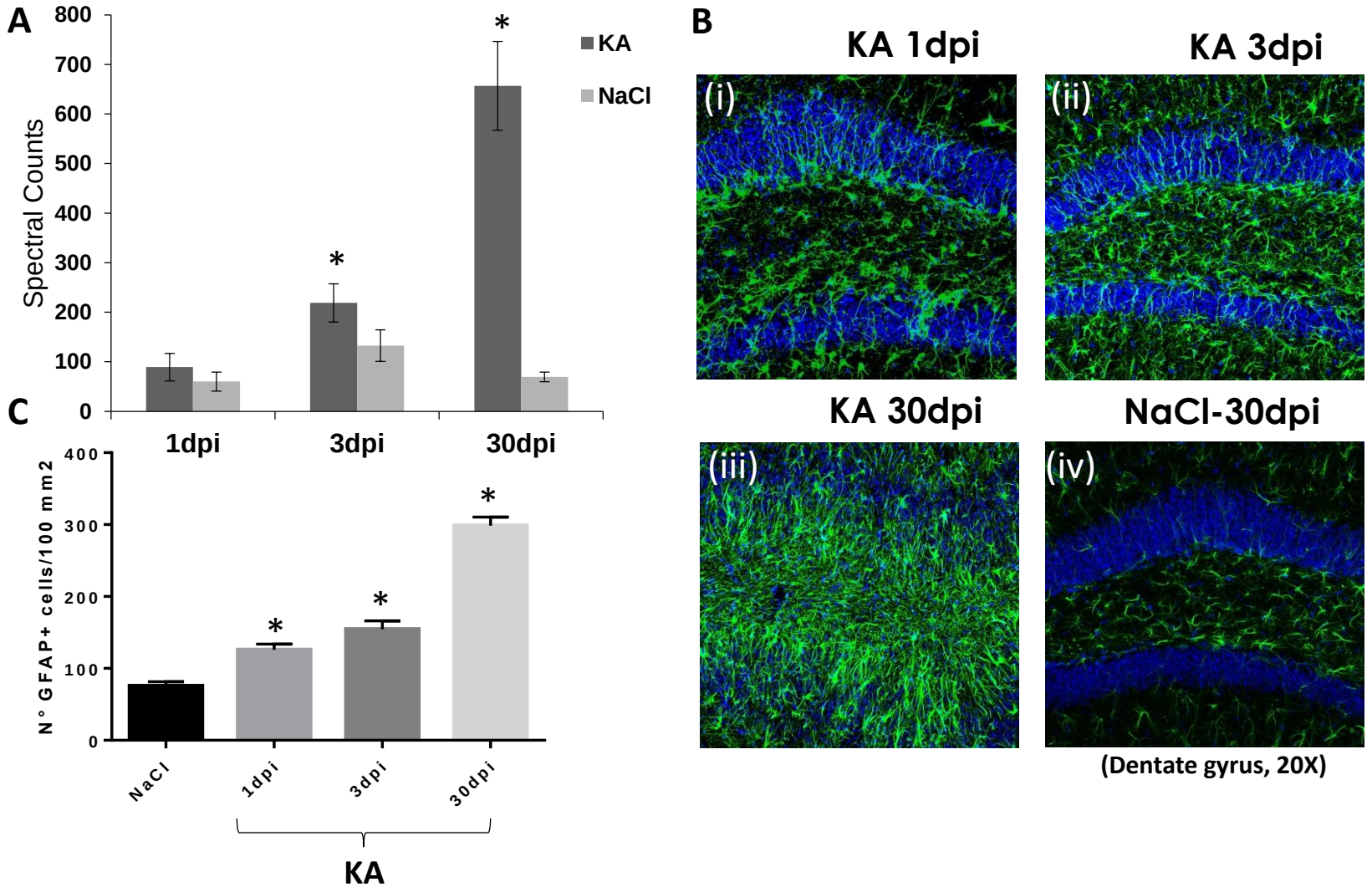
A
Spectral Counts
800
700
600
500
400
300
200
100
0
KA
NaCl
1dpi
3dpi
30dpi
B
KA 1dpi
KA 3dpi
KA 30dpi
NaCl-30dpi
(i)
(ii)
(iii)
(iv)
(Dentate gyrus, 20X)
C
N° GFAP+ cells/100 mm2
400
300
200
100
0
NaCl
1dpi
3dpi
30dpi
KA

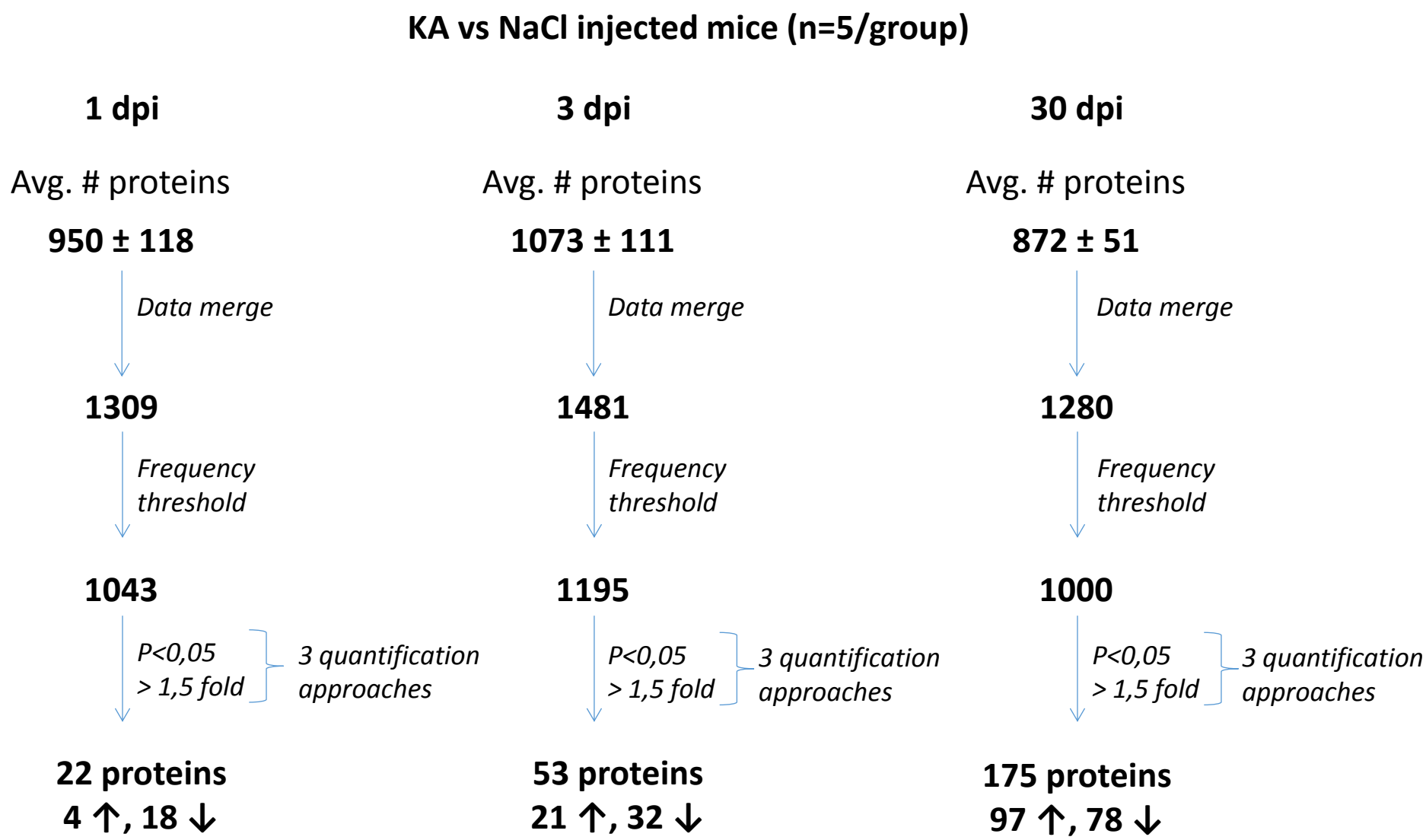
KA vs NaCl injected mice (n=5/group)
1 dpi
Avg. # proteins
950 ± 118
Data merge
1309
Frequency threshold
1043
P<0,05
> 1,5 fold
3 quantification approaches
22 proteins
4 ↑, 18 ↓
3 dpi
Avg. # proteins
1073 ± 111
Data merge
1481
Frequency threshold
1195
P<0,05
> 1,5 fold
3 quantification approaches
53 proteins
21 ↑, 32 ↓
30 dpi
Avg. # proteins
872 ± 51
Data merge
1280
Frequency threshold
1000
P<0,05
> 1,5 fold
3 quantification approaches
175 proteins
97 ↑, 78 ↓

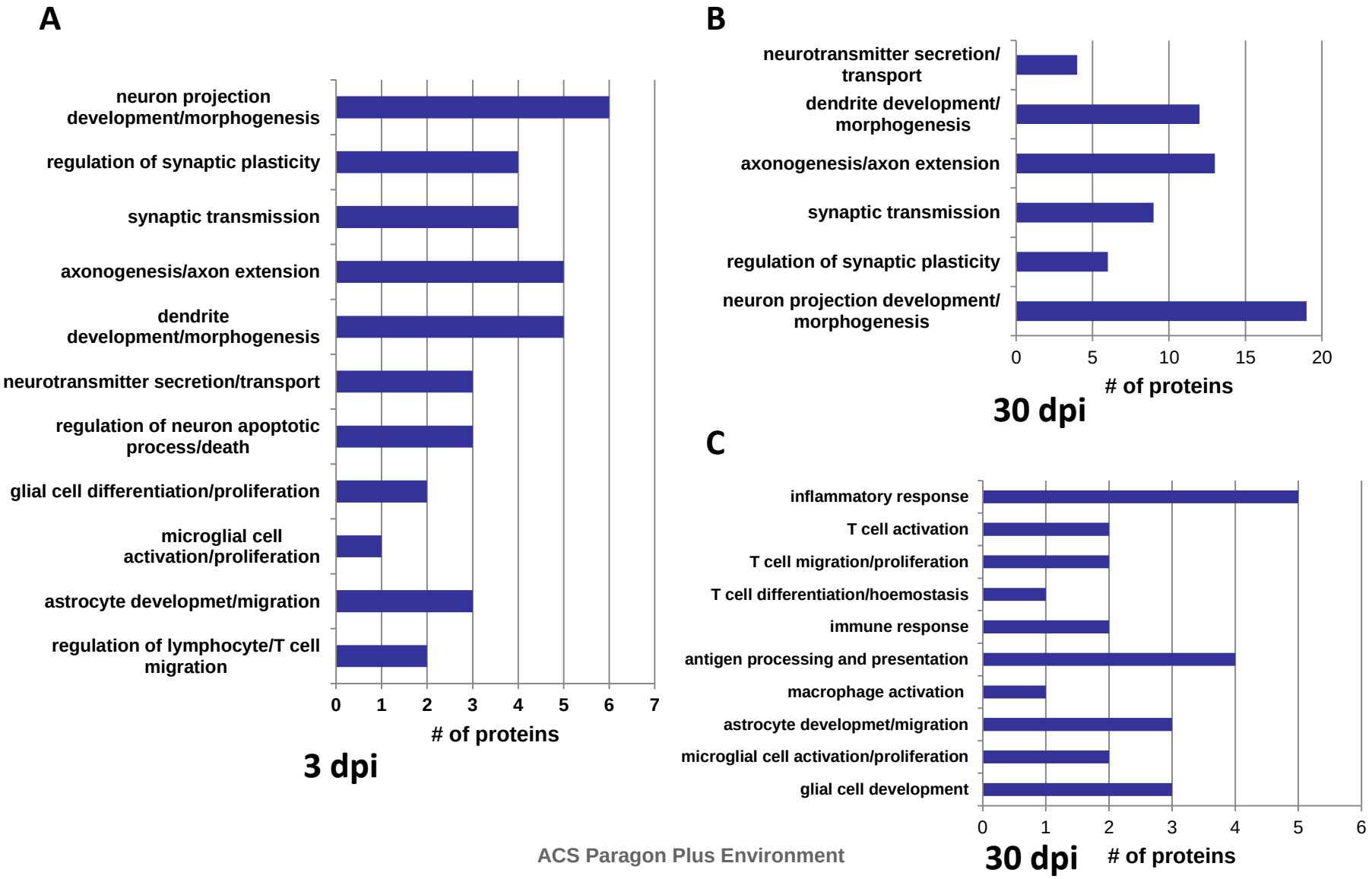
A
neuron projection development/morphogenesis
regulation of synaptic plasticity
synaptic transmission
axonogenesis/axon extension
dendrite development/morphogenesis
neurotransmitter secretion/transport
regulation of neuron apoptotic process/death
glial cell differentiation/proliferation
microglial cell activation/proliferation
astrocyte developmet/migration
regulation of lymphocyte/T cell migration
0 1 2 3 4 5 6 7
# of proteins
3 dpi
B
neurotransmitter secretion/ transport
dendrite development/ morphogenesis
axonogenesis/axon extension
synaptic transmission
regulation of synaptic plasticity
neuron projection development/ morphogenesis
0 5 10 15 20
# of proteins
30 dpi
C
inflammatory response
T cell activation
T cell migration/proliferation
T cell differentiation/hoemostasis
immune response
antigen processing and presentation
macrophage activation
astrocyte developmet/migration
microglial cell activation/proliferation
glial cell development
0 1 2 3 4 5 6
30 dpi
# of proteins

GFAP

ALAAELNQLR

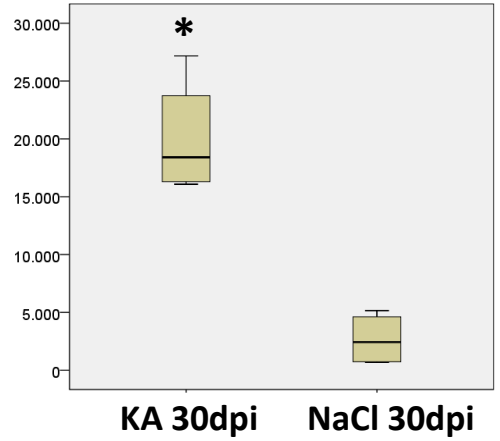

LEAENNLAAYR

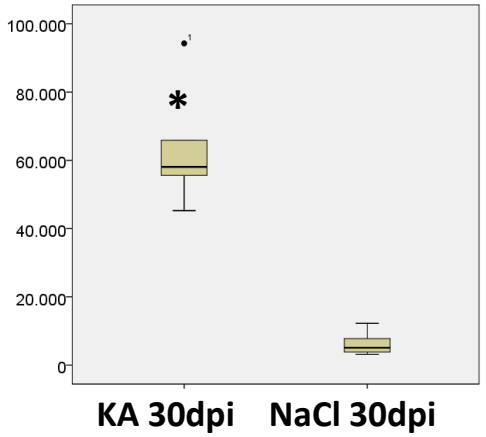

Vimentin

EEAESTLQSFR

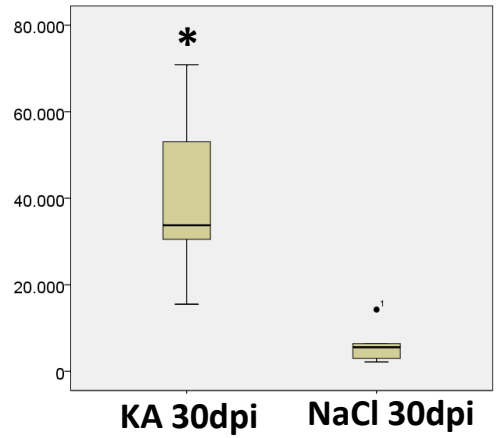

Apolipoprotein E

MEEQTQQIR